Sintering Kinetics of Cr$_2$AlC Powder

A Dissertation Submitted

in Partial Fulfillment of the Requirements for

The Degree of Master of Technology

By

Joshi Ankit Maheshkumar

Under the Supervision of

Dr. Bharat B. Panigrahi

भारतीय प्रौद्योगिकी संस्थान हैदराबाद
Indian Institute of Technology Hyderabad

Department of Materials Science and Metallurgical Engineering

Indian Institute of Technology Hyderabad

July, 2014

Declaration

I declare that this written submission represents my ideas in my own words, and where others ideas or words have been included, I have adequately cited and referenced the original sources. I also declare that I have adhered to all principles of academic honesty and integrity and have not misrepresented or fabricated or falsified any idea/data/fact/source in my submission. I understand that any violation of the above will be a cause for disciplinary action by the Institute and can also evoke penal action from the sources that have thus not been properly cited, or from whom proper permission has not been taken when needed.
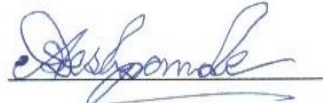
_____
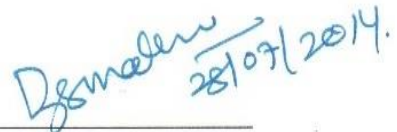
Joshi Ankit Maheshkumar

MS12M1004

Approval Sheet

This thesis entitled *Sintering Kinetics of Cr₂AlC Powder* by Joshi Ankit Maheshkumar is approved for the degree of Master of Technology from IIT Hyderabad.

Dr. Atul Suresh Deshpande

Assistant Professor, Dept. of MSME

Examiner

Dr. Bharat Bhooshan Panigrahi

Assistant Professor, Dept. of MSME

Supervisor

28/03/2014.

Dr. Bhabani Shankar Mallik

Assistant Professor, Dept. of Chemistry

Chairman

Acknowledgements

Dedicated

to

My Father

Mahesh P. Joshi

&

My Mother

Rajni Joshi

Abstract

Cr_2AlC is one of the important member of MAX phase group. Sintering kinetics of freshly synthesis Cr_2AlC ternary carbide powder has been studied using dilatometric sintering methods. Dilatomertic data showed that onset of sintering of Cr_2AlC powder was about 1180 ^0C. There was a distinct change in the sintering rate at about 1315 ^0C. Non-isothermal sintering kinetics of Cr_2AlC powder were analyzed for different sintering mechanisms. Two different sintering models, i.e., Young & Cutler's model and Johnson's model were employed to estimate the diffusion parameters such as diffusion coefficients and activation energies. The estimation of diffusion coefficient were carried out for a range of particle sizes. Attempts were made to study the effect of sintering aids on the densification behavior of Cr_2AlC powder. Various amount of Zr powder was used as sintering aid. It was noticed that large amount of Zr caused expansion on the compact, Very small amount of Zr powder may be helpful to enhance the sintering of Cr_2AlC.

Contents

Chapter 1

Introduction

1.1   Introduction

MAX phases are nano-layered ternary carbides with general formula of $M_{n+1}AX_n$ (n = 1-3), where M is an early transition metal, A is a group IIIA or IVA element and X is either carbon or nitrogen.[1] These materials have unique combination of properties of both ceramics and metals with exceptional combination of mechanical, electrical and thermal properties. Similar to ceramics, they have low density, low thermal expansion coefficient, high modulus, high strength and good oxidation resistance at high temperature. They are good electrical and thermal conductors, easily machinable and have good thermal shock resistances like metals [1]. Due to these unique combination of attractive properties they are promising candidate for diverse field of applications, especially as high temperature materials, protective coatings, materials for lead-cooled reactors and electrical contact materials [2]. The MAX phases crystallize in hexagonal structure with space group of $P6_3/mmc$. Up to now, more than 60 members of MAX phases have been discovered to be thermodynamically stable. Depending on the value of n, MAX phases have been categorized into 3 major groups: i.e. M_2AX (211 phase), M_3AX_2 (312 phase) and M_4AX_3 (413phase). Some of the members such as Ti_3SiC_2, Ti_3AlC_2, Ti_2AlC and Cr_2AlC are among the well investigated. Figure 1.1 (a), (b) and (c) demonstrates the crystal structure of 211, 312 and 413 phases respectively [1].

Nearly close-packed M-layer is interleaved by the A-layer, and the X-atoms filling the octahedral sites of M-layers. Similar to rock salt structure, M_6X octahedral are edge sharing. The A-group atoms are located at the center of trigonal prisms, larger than octahedral sites so that, it can accommodate the larger A-atoms [3]. The main difference in structures as shown in Figure 1.1 is the number of M layers separating the A layers: in the 211 phase, there are two; in the 312 phase, there are three; and in the 413 phase, there are four. Bonding in the MAX phases is a combination of metallic, covalent and ionic. Like MX compounds, there is a strong overlap between the p-levels of the X atoms and the d-levels of the M atoms, leading to strong covalent bonds. The p-orbitals of A-atoms overlap

the d-orbitals of the M-atoms, leads to metallic M-A bonding. In the M_2AlC phases, there is a net transfer of charge from the A to the X atoms [3, 38].
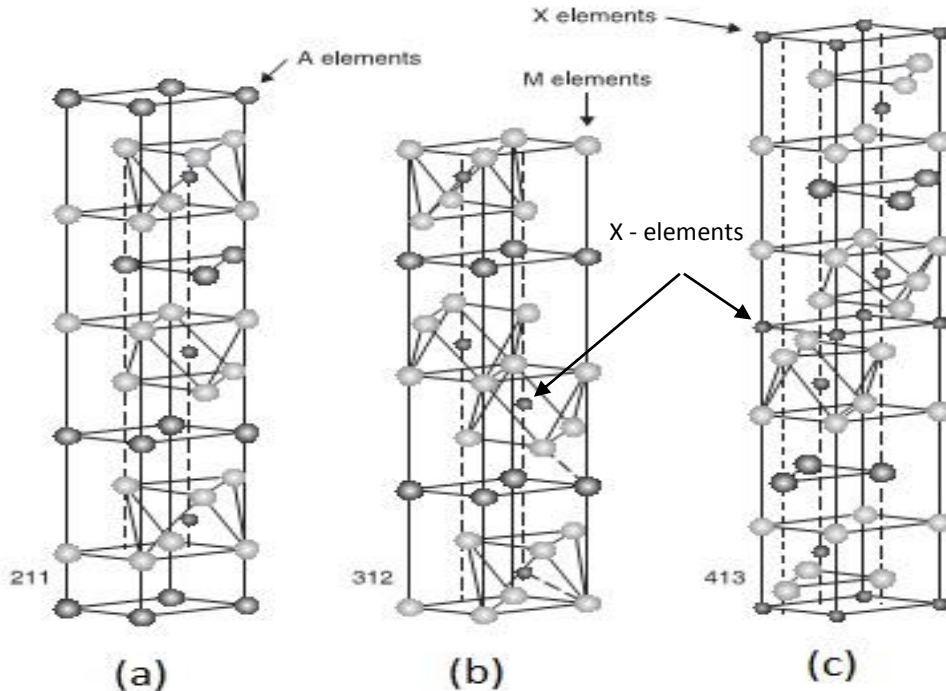

Figure 1.1: Crystal structure of 211 (a), 312 (b) & 413 (c) MAX phases respectively. [2]

Some of the early MAX phase compounds were initially synthesized in powder form, more than 35 years ago by H. Nowotny. Although little was known about their properties until 1996 when Barsoum group got breakthrough in synthesis of high purity bulk Ti_3SiC_2 [4]. The bulk and powder samples of these compounds are generally produced by solid-solid or solid-liquid reactions by using elemental powders or by some intermediate carbides. Although MAX phases have many potential applications, obtaining monolithic is a prerequisite before they can be used in industry.

1.2 Cr_2AlC

At present date, Cr_2AlC (CAC) is one the most studied compound among all the MAX phases after Ti_3SiC_2 and Ti_3AlC_2 [5]. CAC is the only stable ternary carbide in Cr-Al-C system and was first discovered by Jeitschko et al. [6] in 1980s. Stoichiometric CAC involves 72.7 wt. % Cr, 18.9 wt. % Al and 8.4 wt. % C [7]. Figure 1.2(a) shows the crystal structure of CAC. As shown in Figure 1.2 (b), stacking sequence of Cr and Al layer along

the [0001] direction is A$\underline{B}$AB$\underline{A}$B where the underlined letters refer to Al layer [8]. The carbon atoms occupy the interstitial sites of Cr octahedral as shown in Figure 1.2 (c). Lattice parameters of CAC are $a = 2.858$ Å, and $c = 12.818$ Å respectively.

| (a) | (b) | (c) |
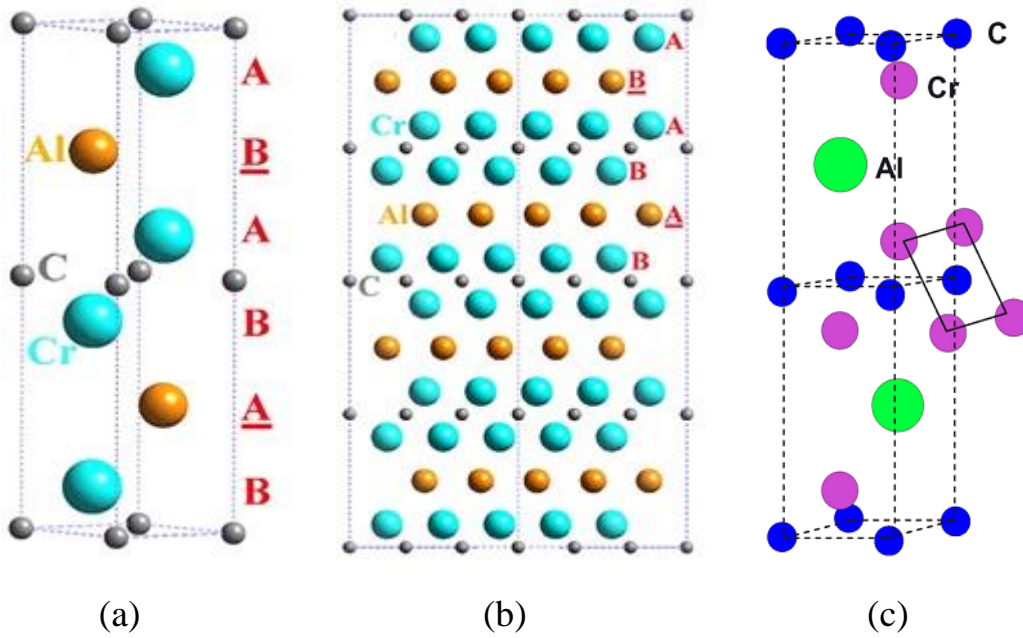
Figure 1.2: (a) Crystal structure of CAC, (b) arrangement of atoms on a (1210) plane and (c) position of C atoms in Cr octahedral. [8, 11]

Table 1.1: Properties of Cr_2AlC[2, 5, 10, 11, 39]

Lattice parameter (Å)	a = 2.86, c = 12.82
Density (g/cm^3)	5.1 - 5.24
Vickers hardness (GPa)	5.5 ± 0.4
Young's Modulus (GPa)	288
Flexural Strength (MPa)	483
Compressive Strength (MPa)	1159
Electrical resistivity (μΩm)	0.71 - 0.74
Thermal expansion coefficient (K^{-1})	1.26 X 10^{-05}

Ab initio calculation and experimental investigation indicates that CAC has 11 % larger bulk modulus than Ti_3SiC_2, exhibits relatively higher hardness, better corrosion-oxidation resistance then other MAX phases. Good high temperature oxidation resistance and hot corrosion resistance is attributed to the formation of protective alumina scale [1, 9]. Few important physical properties of CAC have been tabulated in Table 1.1. High density parts of CAC were produced by elemental powders of Cr, Al & C mostly through hot pressing or sintering under applied pressure, including spark plasma sintering and pulse discharge sintering. Producing a high-density parts through pressureless sintering [5] is a breakthrough in the technological as well as economical point of view and also enhance the application area of this compound. At the same time, to achieve maximum of theoretical bulk density is always desirable for powder-metallurgical parts for load bearing and mechanical applications.

Sintering is a process in which particles bond together when heated to a sufficiently high temperature. The driving force is the net reduction in the surface energy. Liquid-phase sintering (LPS) involves the formation of a liquid phase to promote higher densification rates and lower the sintering temperatures. There are two main forms of LPS. When a liquid phase is obtained by melting of powder mixture and is persistent throughout the high-temperature portion of the sintering cycle, the process is termed as persistent LPS. In some systems with a low inter-solubility even in the presence of a persistent liquid, an activator can be used to enhance sintering. This is termed as activated liquid-phase sintering (ALPS). Alternatively, transient liquid-phase sintering (TLPS) involves liquid that disappears due to dissolution into the solid or formation of a new phase/compound [12].

Referring to the Cr-Zr phase diagram, as shown in Figure 1.3, chromium has almost negligible solubility for zirconium, while β-zirconium can dissolve more than about 7 wt.% chromium at the eutectic temperature of 1332 ^{0}C. This type of solubility characteristics is one of the essential criteria for designing the sintering aids. Due to this eutectic point of composition of Zr –14 wt.% Cr at 1332 ^{0}C, there is a strong possibility for the formation of liquid phase during the sintering cycle. By adding very small amount of Zr in CAC, transient liquid phase sintering might be expected.
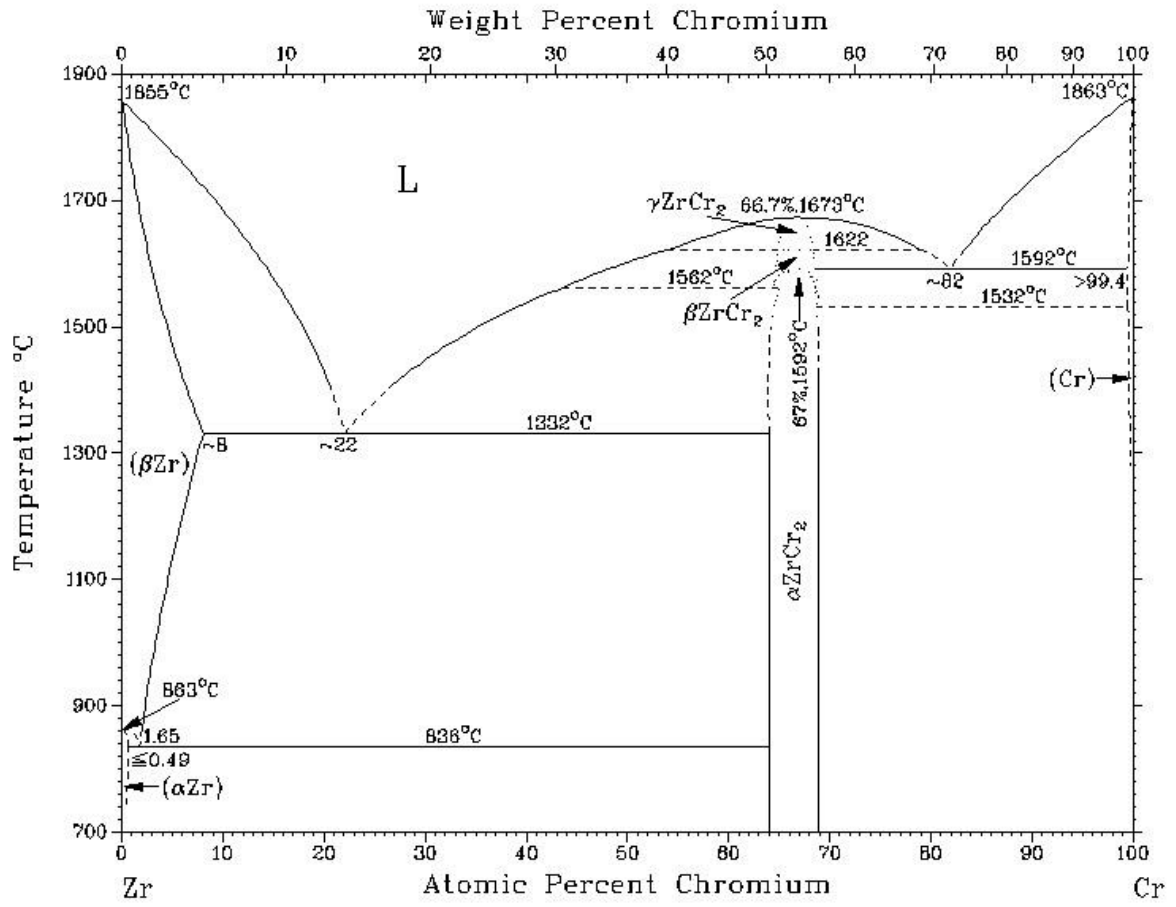
Figure 1.3: Zr-Cr Phase Diagram. [13]
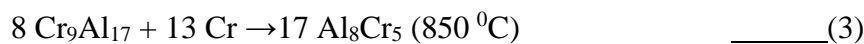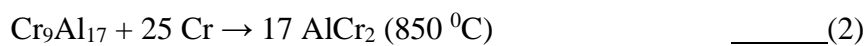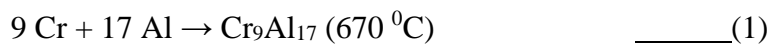
Chapter 2

Literature Review

MAX phases can be made directly from starting materials by in situ synthesis or reacting sintering, which combine the synthesis reaction and densifying process. The solids can also be made by only the densifying process from pre-made MAX-phase powders. The powders can be made directly in powder form or by breaking partially sintered porous samples [14]. Moreover thin film and coatings of MAX phase have also been developed by physical vapor deposition (PVD), chemical vapor deposition (CVD) and thermal spray (TS).

Barsoum and group [16] fabricated bulk polycrystalline Ti_3SiC_2 using 3Ti/SiC/C powders through hot isostatic pressing. The powders were cold-pressed at the applied pressure of 180 MPa and then HIPed 1600 °C for 4 hours. Flexible container dies are used in HIP with isotropic pressurization. Consolidation of powder container occurs in internally heated pressure vessel. High pressure gas i.e. argon or nitrogen, is used to transfer heat and pressure to the compact. There was less than 1 vol. % SiC and TiC in the final product. Later, Barsoum et al. [17] successfully synthesized Ti_3AlC_2 from Ti, Al_4C_3 and graphite mixture by HIP at 1400 °C for 16 hours. The samples were predominantly single phase, fully dense with containing about 4 vol.% Al_2O_3 as an impurity. Encouraged by the success of obtaining pure Ti_3SiC_2 and Ti_3AlC_2, they subsequently fabricate many other MAX phases, such as Ti_4AlN_3, Ta_2AlC, Ti_2InC, Zr_2InC, Hf_2PbC, Zr_2PbC and V_2AlC [2]. In that way HIP was a breakthrough for fabricating pure bulk MAX phases. Zhou et al [18] developed an in-situ hot pressing / solid–liquid reaction synthesis to fabricating monolithic MAX phases in a short time which saves considerable energy with large-scale samples. Hot pressing (HP) is the stress enhanced densification process [15]. The die is usually made up from graphite to allow external induction heating. Sun et al. [19] adopted in-situ HP / solid–liquid reaction to fabricate Ti_3SiC_2. Spark plasma sintering (SPS) [22] provides a very quick heating, and has been widely used to fabricate wide verity of bulk polycrystalline materials. SPS utilizes uniaxial force and ON-OFF DC pulse energizing. The ON-OFF DC pulse voltage and current creates spark discharge and Joule heat points between material particles i.e., high-energy pulses at the point of inter-granular bonding. The high frequency transfers and disperses the spark/Joule heating phenomena throughout the specimen,

resulting in a rapid and thorough heat distribution, high homogeneity and consistent densities. Gao et al [23] synthesized and simultaneously consolidated Ti_3SiC_2 from the starting mixture of Ti/Si/2TiC by SPS at 1200 °C. They have reported that the final compositions could be tailored by adjusting the process parameters. Zhu et al [24] studied the effect of aluminium on synthesis of Ti_3SiC_2 by SPS from Ti, Al, Si and C elemental powders and shows that proper addition of Al not only favored the formation but also accelerated the crystal growth of Ti_3SiC_2. Bulk Ti_3SiC_2 material with high purity and density could be obtained by SPS from the elemental powder mixture with starting composition of $Ti_3Si_{1-x}Al_xC_2$, where x = 0.05–0.2. Zhou et al. [25] obtained dense Ti_2AlC from 2Ti/1.2Al/C mixture at 1100 °C and 30 MPa for 1 hour by SPS. Synthesis of pure MAX-phase powders is more important because powders are essential for fabricating complex shapes and composite bulk materials. Pressureless sintering (PS) is a conventional powder metallurgy route, where sintering of a green compact is carried out without application of mechanical pressure. The advantages of PS are simple devices, low cost, easy to make mass production and good control over purity and particle size. Sun et al [19] have reported synthesize of Ti_3SiC_2 powder by pressureless sintering. Single phase Ti_3SiC_2 has been obtained by heating Ti, Si, and TiC powders with a composition of Ti/1.10Si/2TiC. It was found that adding 10 % excess Si is essential for preparation of Ti_3SiC_2 because Si evaporates at high temperature.
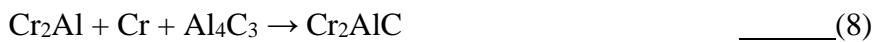
Zhijun et al. [7] have synthesized bulk Cr_2AlC by in-situ HP/ solid-liquid reaction method using Cr, Al and graphite elemental powders as starting materials. The relative density of the as-synthesized sample was 95 %. This was the earliest attempt for the bulk sample synthesis of CAC. They observed small amount of Cr_9Al_{17}, Al_8Cr_5 and $AlCr_2$ impurities. The whole reaction process explained with following equations:

$$9\,Cr + 17\,Al \rightarrow Cr_9Al_{17}\,(670\,^0C) \qquad \underline{\qquad}(1)$$
$$Cr_9Al_{17} + 25\,Cr \rightarrow 17\,AlCr_2\,(850\,^0C) \qquad \underline{\qquad}(2)$$
$$8\,Cr_9Al_{17} + 13\,Cr \rightarrow 17\,Al_8Cr_5\,(850\,^0C) \qquad \underline{\qquad}(3)$$
$$Al_8Cr_5 + 11\,Cr + 8\,C \rightarrow 8\,Cr_2AlC\,(1050\,^0C) \qquad \underline{\qquad}(4)$$
$$AlCr_2 + C \rightarrow Cr_2AlC\,(1050\,^0C) \qquad \underline{\qquad}(5)$$

Looking at the thermodynamic studies of Cr-Al-C ternary phase diagrams, Nowotny et al. [6] reported that at 1000 ^0C Cr_2AlC is in equilibrium with Al_4C_3, Al_4C_3, γ-Cr_5Al_8, Cr (solid

solution with Al), Cr_7C_3, and Cr_3C_2. At 800°C, Cr_2AlC coexists also with graphite and β-Cr_2Al. Hallstedt et al. [20] has reported that Cr_2AlC is the only ternary phase in Cr-Al-C system. Cr_2AlC melts incongruently at about 1500 ^{0}C to form Cr_7C3 (or Cr_3C_2) and Al_4C_3 with some amount of liquid. Tian et al [21] reported phase formation sequence of Cr_2AlC ceramics starting from Cr-Al-C powders, from the hot pressed specimen at 20 MPa in argon atmosphere in the temperature range of 850-1450 ^{0}C. They found Cr_5Al_8, Cr_2Al and Cr_7C_3 as an intermediate phases during initial heating process. Cr_2AlC forms gradually with increase in temperature at the expense of these intermediates and unreacted Cr and C, and finally reaches to the maximum purity at around 1250 ^{0}C. Up to now, the in-situ HP / solid–liquid reaction synthesis is one of the most effective and practical techniques for the fabrication of monolithic and dense MAX phases. Later Tian et al. [26] have used SPS method to synthesis bulk CAC samples starting with elemental powders. They used two kinds of starting powders; coarse and fine particle size, and obtained density of around 5.12-5.14 g/cm^3 with some impurities of $AlCr_2$ and Cr_7C_3 in the end product. Same author have also reported synthesis reaction of Cr_2AlC from $Cr-Al_4C_3$-C [27] by pulse discharge sintering (PDS). PDS were carried out in vacuum for the temperature range of 850-1350 ^{0}C. It has been presumed that Cr_2AlC phase formed near Al_4C_3 particles by the diffusion of Cr and its reaction with Al_4C_3. Corresponding reactions occurring in the temperature range of 850-1050 ^{0}C were explained as follows:

$$Cr + Al_4C_3 \rightarrow Cr_2AlC + Cr_2Al \qquad \qquad (6)$$

$$Cr_2Al + C \rightarrow Cr_2AlC \qquad \qquad (7)$$

$$Cr_2Al + Cr + Al_4C_3 \rightarrow Cr_2AlC \qquad \qquad (8)$$

With the increasing temperature, Cr_2AlC becomes the major phase with the small amount of impurity of Cr_7C_3.

$$Cr_2Al + Cr + Al_4C_3 \rightarrow Cr_2AlC + Cr_7C_3 \qquad \qquad (9)$$

SPS and PDS are an expensive techniques and can only fabricate small scale samples, accordingly they are mainly employed at the laboratory scale. Some other work has been reported in which pulse discharge sintering, hot pressuring of mechanically activated HP as well as pressured-assisted self-propagating high-temperature synthesis (PSHS) has been employed for the bulk sample preparation of Cr_2AlC and other MAX phases [2, 14].

Tian et al [28] reported a unique molten salt method for Cr_2AlC powder preparation using NaCl-KCl salt mixture at their eutectic composition. They used Cr-Al-C (2:1:1 & 2:1.1:1) elemental powder mixture and mixed them with salt mixture in 2:1, 1.1 and 1:2 powder to salt ratio and heated them in vacuum using quartz tube. Cr_2AlC powder with 4-7 μm particle size were produced at 1000 ^{0}C while using 1:1 powder to salt ratio. Panigrahi et al. [29, 30] reported powder synthesis of Ti_3AlC_2 and Ti_3SiC_2 via a new route that consist of two-step process. In both the cases, TiC_x powder was synthesized first, which reacts subsequently with Al and Si in the second step to get Ti_3AlC_2 and Ti_3SiC2 powders respectively. Two step process have some advantages like better control over purity and grain size. Same authors have reported similar work for CAC [5] powder synthesis and subsequently by pressureless sintering and 95.7 % dense CAC bulk sample was achieved. Here also two-step process was adopted for CAC powder synthesis in which reaction between previously synthesized CrC_x and elemental Al was carried out. This was one the earliest report on pressureless sintering of CAC powder for the bulk sample preparation. The major reactions were explained as follows:

In first step, while ignoring small amount of Cr_2C,

$$10\ Cr + 5\ C \rightarrow Cr_3Cr_2 + Cr_7C_3 \qquad\qquad (10)$$

And in second step:

$$Cr_3Cr_2 + Cr_7C_3 + 5\ Al \rightarrow 5\ Cr_2AlC \qquad\qquad (11)$$

Recently, Zhongliang et al [31] reported almost similar method of pressureless sintering starting from Cr-Al-C elemental powder instead of two step process. Cr:Al:C powder in the ratio of 2:1.05:1 were taken and sintered at 1350 ^{0}C for 30 minutes of shocking time. High purity (97.2 wt. %) Cr_2AlC powder with very small amount of Cr_7C_3 had been synthesized. Following reaction mechanism were proposed:

At 900 -1000 ^{0}C:

$$5\ Cr + 8\ Al \rightarrow Cr_5Al_8 \qquad\qquad (12)$$

$$2\ Cr + Al \rightarrow Cr_2Al \qquad\qquad (13)$$

$$Cr_5Al_8 + 13\ Cr + Al \rightarrow 9\ Cr_2Al \qquad\qquad (14)$$

At 1100-1250 ^{0}C:

$$Cr_2Al + C \rightarrow Cr_2AlC \qquad\qquad (15)$$

$$7\ Cr + 3\ C \rightarrow Cr_7C_3 \qquad\qquad (16)$$

Advancing further in their paper, Panigrahi et al. [29, 30] also reported Nickel assisted sintering and enhancement of density of Ti_3AlC_2 and Ti_3SiC_2 powder under pressureless condition. Nickel is known for its higher diffusivity in titanium and was found to enhance the sintering rate of titanium. It also suppressed the grain coarsening process up to certain extent during sintering. By addition of Ni, relative density of 97.6 % and 98.5 % were achieved for Ti_3AlC_2 and Ti_3SiC_2 respectively. Also some elementary work to predict the diffusion parameters [32] of Cr_2AlC and Ti_3SiC_2 were reported. Johnson model was applied to non-isothermal sintering data; and volume and grain boundary activation energies were estimated. This is the only reported work available on the sintering kinetics of CAC powder. Hence there is a scope to further investigate the sintering kinetics of CAC and to estimate the physical parameters i.e., diffusion coefficient and activation energy. Application of some other models also helps to compare the different outcomes. Also the sintering kinetics of CAC has not been reported as per best of our knowledge. Hence the effect of sintering aid on the sintering behavior of CAC powder is the area in which one can focus. So as already outlined, after going through different Cr based binary phase diagrams, effect of Zr as a sintering additive needs to be explored more.

Following objectives have been setup for the present work.
- **To study the sintering kinetics of Cr_2AlC powder during non-isothermal sintering.**
- **To study the effect of little amount of Zr addition on sintering behaviour and microstructure of Cr_2AlC powder.**

Chapter 3
Experimental Procedure

3.1 Synthesis of Cr$_2$AlC Powder

Cr$_2$AlC powder synthesis has been carried out by two step process [5] in the present work. In the first step CrC$_x$ (x=0.5) powder was produced from elemental Cr (99.5 %, -325 mesh, Alfa Aesar) and graphite (99 %, 7-11 μm, Alfa Aesar) powders. Cr:C has been taken in 2:1 mole ratio and mixed by turbo mixture using toluene as a mixing medium. The dried mixture was heated in tubular furnace with flowing Argon atmosphere at 1350 ^{0}C for 2 hours. The partially sintered CrC$_x$ was ground in agate mortar-pastel and sieved by -325 mesh screen.

In second step, CrC$_x$ powder mixed with Al (99.5 %, -325 mesh, Alfa Aesar) elemental powder in 2:1.1 mole ratio by using similar method. Dried mixture was heated in the same furnace with flowing Argon at 1250 ^{0}C for 2 hours. Here excess amount of Al was added to compensate the loss of Al due to evaporation at such a high temperature. Partially sintered compact was crushed to fine size powder by agate mortar-pastel, sieved by -325 mesh screen and used for further sintering studies.

3.2 Sintering of Cr$_2$AlC Powder

To prepare pellets of freshly synthesized CAC powder, 4 wt.% binder (paraffin wax) was first dissolved in toluene and then CAC powder was added. After proper mixing and drying, several pallets was prepared from this power by compacting at 40 MPa of applied pressure using 7 mm diameter cylindrical steel die and punch. Also to study the effect of sintering-aid, 1, 2 & 5 wt. % Zr has been added in CAC powder and pellets were prepared by similar method (CAC-1Zr, CAC-2Zr & CAC-5Zr).

Sintering of CAC samples were carried out at two different temperatures of 1300 ^{0}C and 1400 ^{0}C on Single push rod Dilatometer (Dilamatic II, Theta Industries US). Similarly dilatometry sintering of CAC-1Zr, CAC-2Zr & CAC-5Zr samples were carried out in identical condition at 1300 ^{0}C. After inserting sample, first of all dilatometer tube were evacuated for 10 minutes followed by purging of Ar for 30 minutes to ensure the inert

atmosphere during sintering. For all the samples, same heating rate of 10 ^{0}C/min with 10 minutes of holding time at 400 ^{0}C was employed to remove the binders before the onset of sintering.

3.3 Characterization

Dimensional and weight measurements of all the green and sintered samples were carried out. Density of all green and sintered samples were calculated from measured weight and volume of each pellets. All as received elemental powders have been characterized by X-ray powder diffractometer (PANalytical X'Pert Pro) with Cu Kα (λ = 1.5456 Å, step size 0.01^0) radiation. Also the constituent phases of both CrC_x & Cr_2AlC powders were analyses using XRD. All sintered samples were characterized by XRD with the help of multi-purpose stage equipped with the same instrument. Care has been taken to ensure the flat upper surface after removal of top layer by polishing to get rid-off oxide layer. The morphology of synthesized Cr_2AlC powder has been observed by scanning electron microscope (FESEM: Carl Zaiss NTS GmbH - Germany). Morphology of the broken surfaces of all the sintered samples have been observed by SEM. Also the elemental mapping and EDX analysis were carried out for selective sintered samples. Differential scanning calorimetric (DSC: NETZSCH DSC 404F3) analysis has also been carried out for different combinations of Cr, Al & C as well as synthesized Cr_2AlC powder and all Zr added CAC-Zr mixed powders.

3.4 Dilatometer Sintering

Push rod dilatometer serve the measurement of the change in length as a function of temperature. Dilatometry is the method for precise measurement of dimensional change of solid compacts at a programmed temperature change and over a range of time with negligible sample strain (ASTM E831, ASTM D 696). Hence dilatometry has been used for the long time to study the sintering behavior of powder compacts. Dilatometer sintering plot can be evaluated in two different region, i.e. non-isothermal part and isothermal. During non-isothermal sintering, temperature is continuously increased at a constant heating rate, while in isothermal sintering temperature is kept constant for the range of time. A schematic presentation of shrinkage measurement method has been shown in figure 3.1. Suppose the sample is expected to show a net expansion of h when the temperature reached T. Then the new length of the sample L_1 at temperature T_1 can be given as L_0 + h,

where L_0 is the sample length at room temperature. For the non-isothermal sintering plot, a straight line of expansion with a constant slope can be plotted parallel to the sintering plot with assumption that the thermal expansion coefficient is constant throughout the temperature range. At higher temperature, just after the onset of sintering dilatometer plot shows a change in slope and gradually slope becomes negative. Shrinkage was measured at each temperature point from the sample length L_n (at temperature T_n), considering thermal expansion. Shrinkage S_a is shown at temperature T_a in figure 3.1. Similarly for isothermal sintering plot, straight line of thermal expansion with zero slope can be obtained. Shrinkage S_b, S_c etc. has been measured in the similar manner from this line at regular interval of time (t_1, t_2 etc.) as shown in figure 3.1.
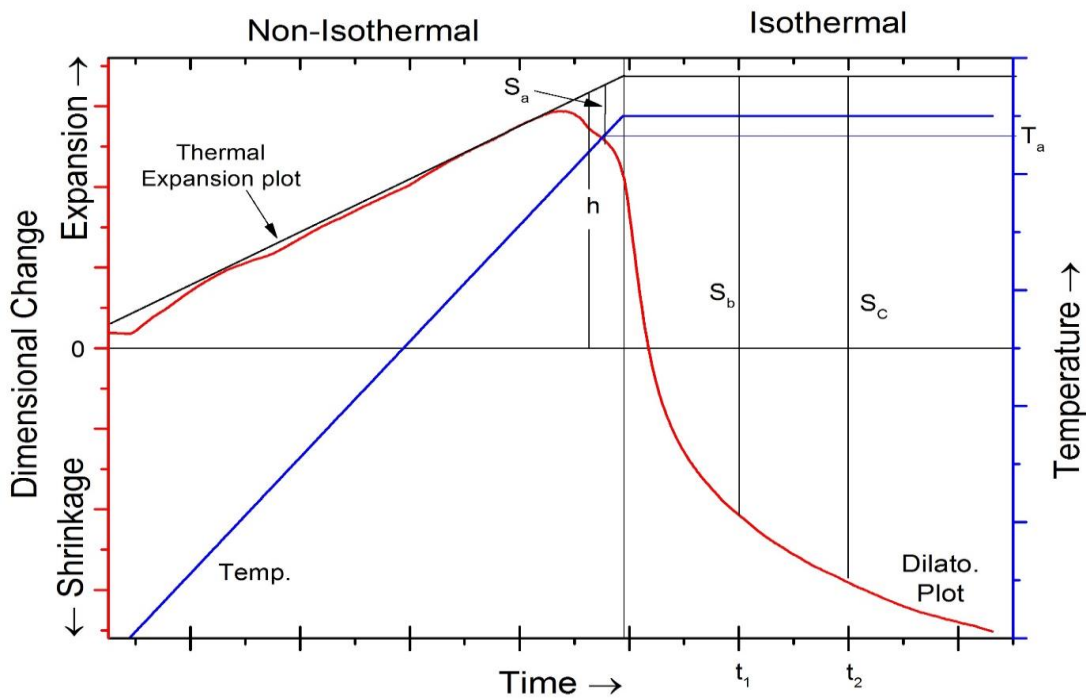
Figure 3.1: Schematic representation of shrinkage measurement from dilatometer plot.

13

Chapter 4

Results and Discussion

4.1 Synthesis of Cr$_2$AlC Powder

Figure 4.1 shows the XRD patterns of as received Cr, Al & graphite powders and have been compared with their standard ICDD (C – 411487, Al – 894037, Cr - 894055) data for the phase identification. Similarly, as synthesized CrC$_x$ and Cr$_2$AlC powders were analyzed as shown in Figure 4.2 and Figure 4.3 respectively. It has been observed that CrC$_x$ mainly consists of three different carbides; namely Cr$_{23}$C$_6$, Cr$_7$C$_3$ and Cr$_3$C$_2$, (ICDD file no. 350783, 361482 & 350804 respectively) whereas Cr$_2$AlC powder was found to be of high purity with negligible amount of Cr$_7$C$_3$ as an impurity. All the peaks of Cr$_2$AlC have been identified and indexed as per the ICDD file no. 892275.
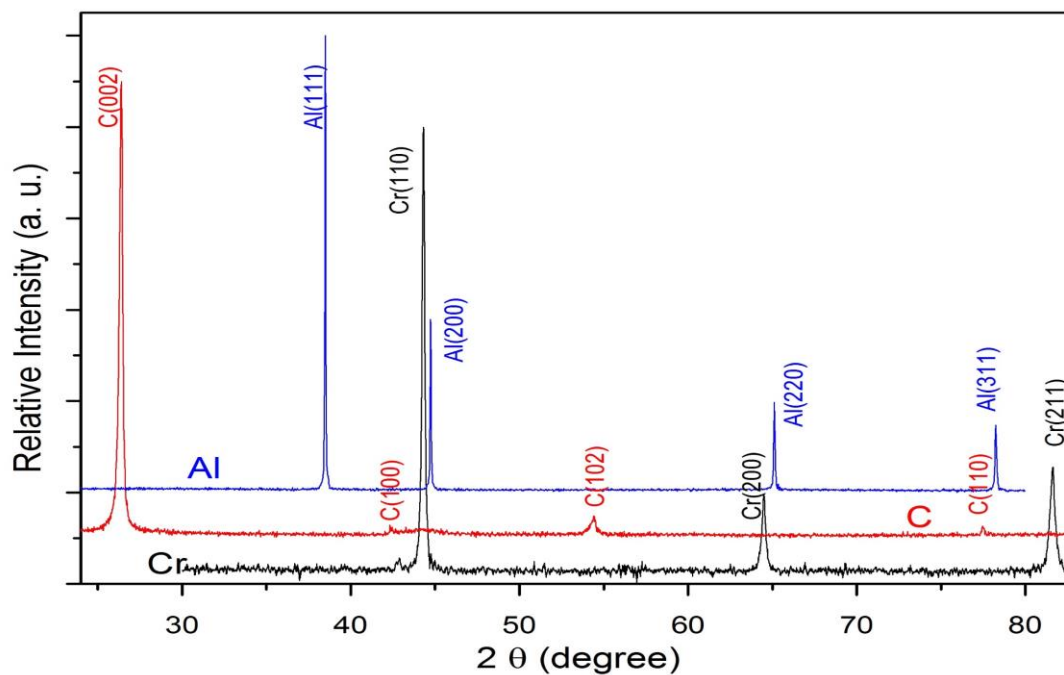
Figure 4.1: XRD patterns of Cr, Al & C elemental powders.

Figure 4.4 (a) and (b) shows the SEM micrograph of Cr$_2$AlC powder, having particle size in the range of 1-20 μm with an average size of about 10 μm. Large amount of agglomerates were observed in the powder as shown in figure 4.4 (c), due to the partial

sintering during the synthesis itself. Also the layered structure can been seen in figure 4.4 (d), an inherent characteristic of MAX phase compounds.
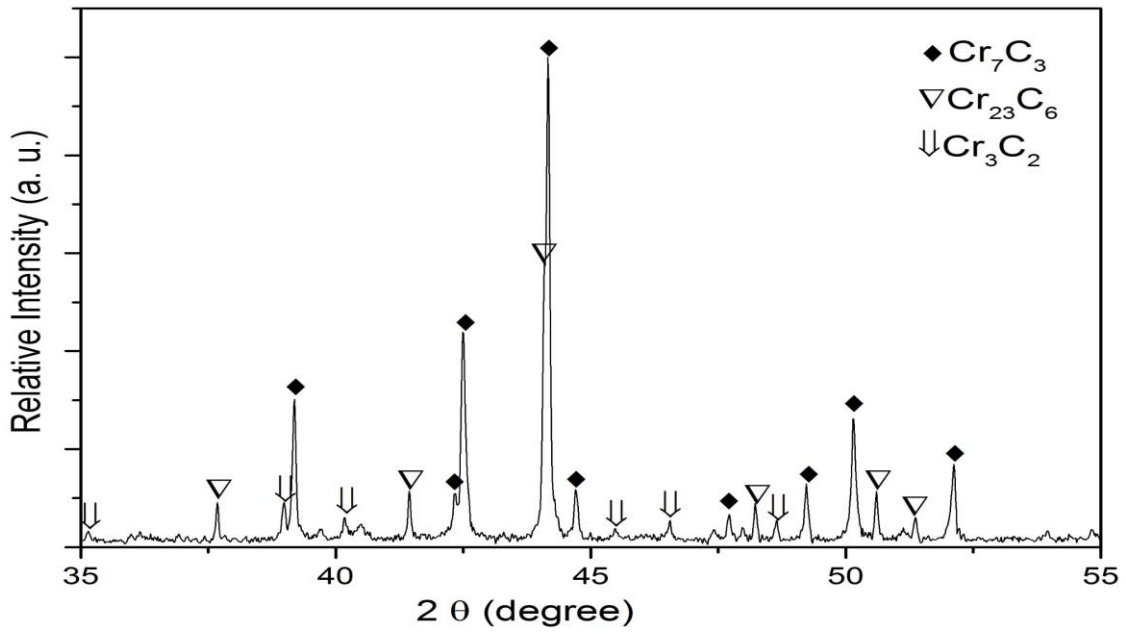
Figure 4.2: XRD pattern of synthesized CrC$_x$ powder.
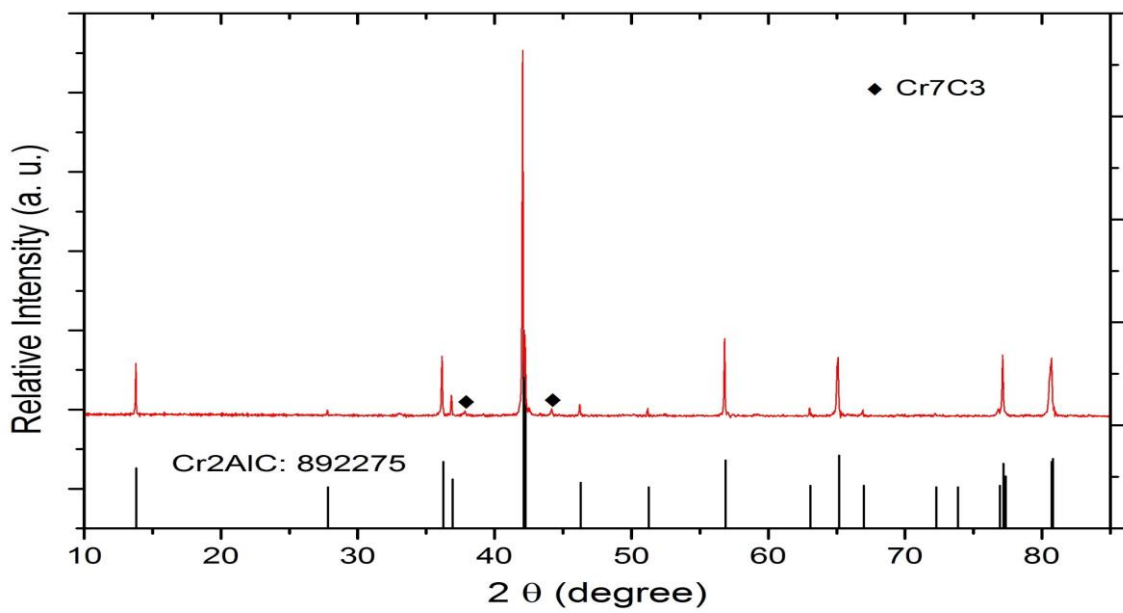
Figure 4.3: XRD pattern of synthesized Cr$_2$AlC powder.
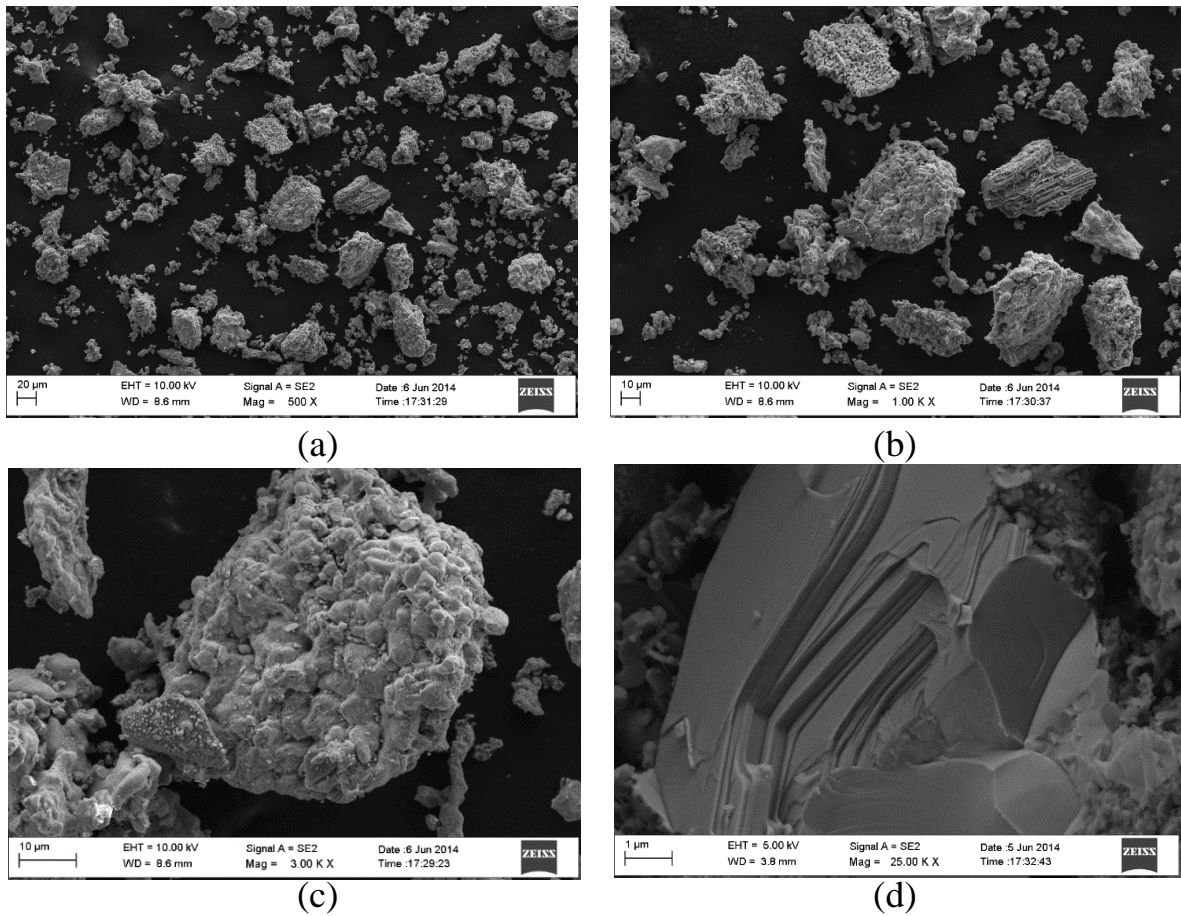
Figure 4-4: SEM micrograph of synthesis Cr_2AlC powder; (a) & (b) shows the wide range of particle size, (c) agglomerated particles and (d) layered structure of CAC.

4.2   Sintering of Cr_2AlC Powder

From some of the previous work reported on the sintering of Cr_2AlC [5, 32], we have decided to start with the sintering temperature of 1300 ^0C. Figure 4.5 shows the dilatometer sintering plot of Cr_2AlC powder compact. Sintering onset temperature was around 1180 ^0C. At about 1315 ^0C there was a significant change in the nature of curve; sintering process seems to be accelerated at this point. Shrinkage in the isothermal region has been measured by the method as already outline in the previous section. Corresponding shrinkage and shrinkage rate as a function of time from t = 0 (beginning of isothermal region) is plotted in Figure 4.6. Shrinkage increases whereas shrinkage rate decreases as a function of time.

Because of the very small region of the non-isothermal section available after the onset of sintering, next sintering was carried out at some higher temperature of 1400 ^0C. Instead of 60 minutes, in this case isothermal shocking time was increased to 120 minutes. As shown

in Figure 4.7, again the sintering onset temperature was 1179 ^{0}C. Corresponding shrinkage and shrinkage rate as a function of isothermal time have been plotted in Figure 4.8. Due to higher temperature, higher shrinkage was observed, with shrinkage rate becomes constant at longer socking time. By enlarging the non-isothermal region as shown in Figure 4.9, abrupt change in slope of sintering plot at around 1315 ^{0}C has been observed. After plotting shrinkage vs temperature for this region, Figure 4.10, slope change was clearly revealed. This is possibly due to the different sintering mechanism active at higher temperature. Therefore non-isothermal shrinkage data has been separately analyzed for two different range of temperatures i.e. 1180-1315 ^{0}C and 1315-1400 ^{0}C.
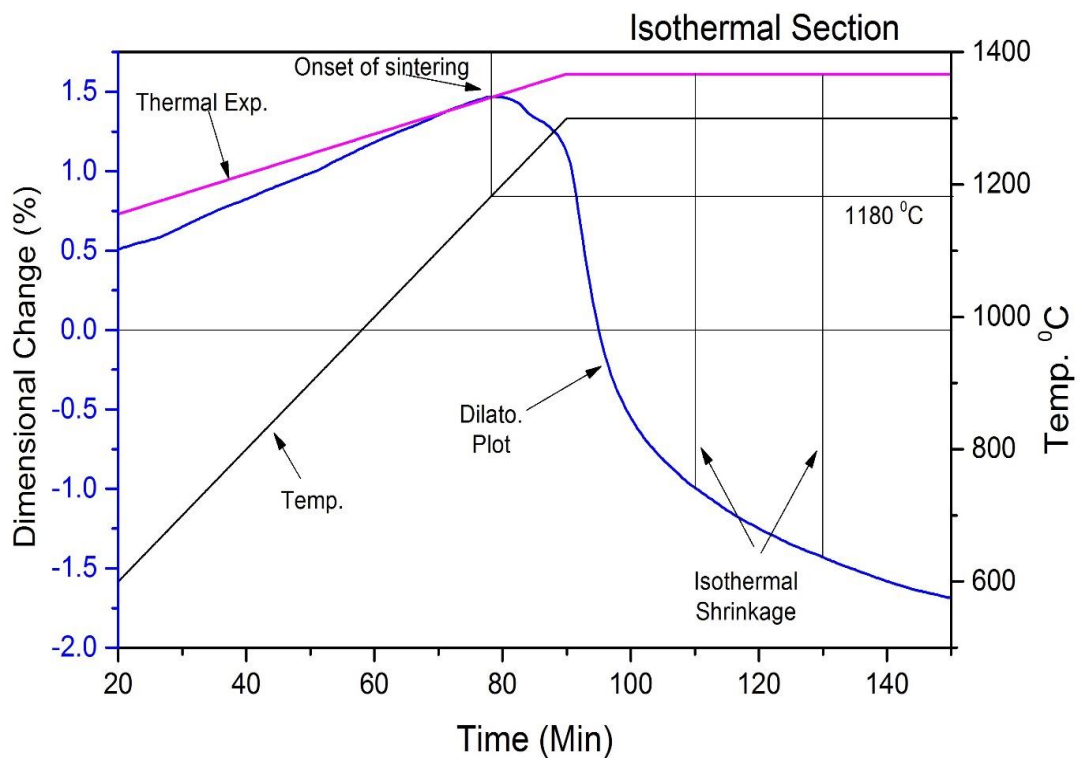
Figure 4.5: Dilatometer plot of the CAC sample sintered at 1300 ^{0}C for isothermal holding of 1 hr.
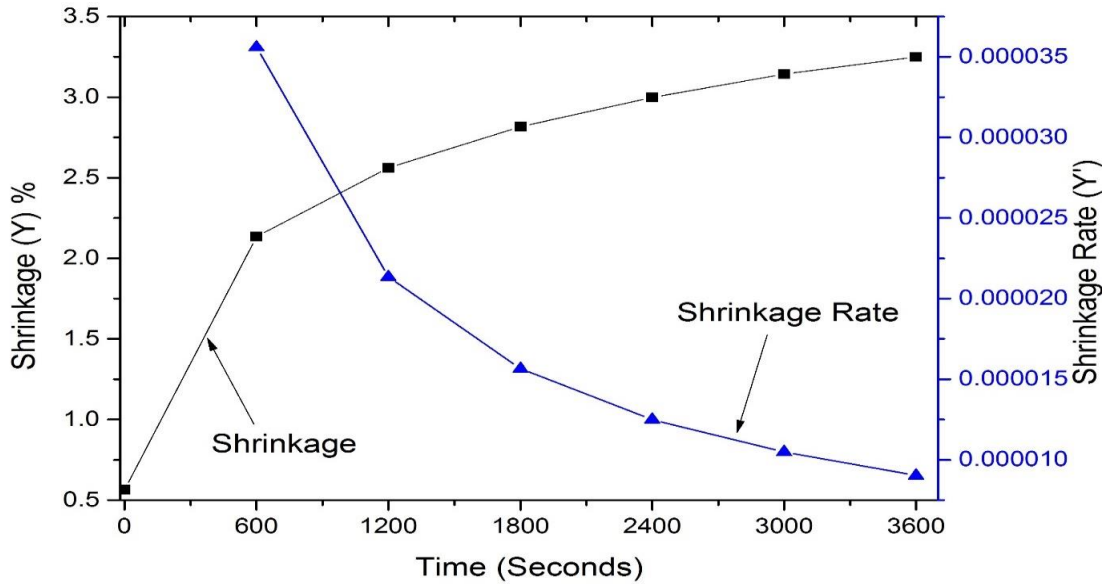
Figure 4.6: Measured shrinkage & shrinkage rate as a function of isothermal holding time at 1300 ^{0}C.
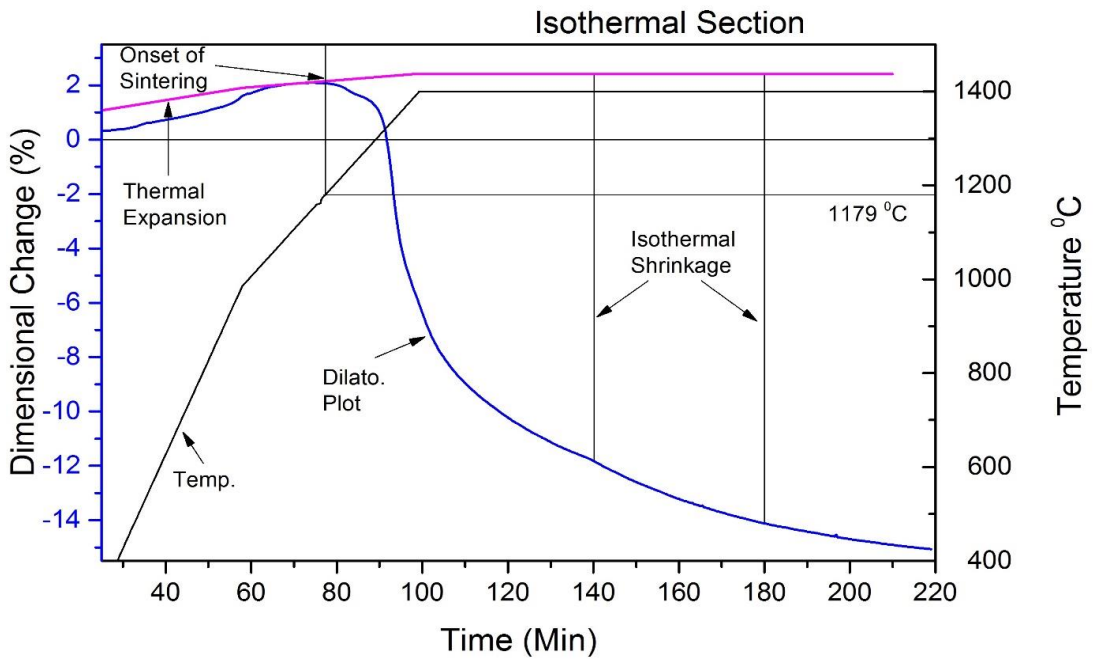
Figure 4.7: Dilatometer plot of the CAC sample sintered at 1400 ^{0}C for isothermal holding of 2 hr.
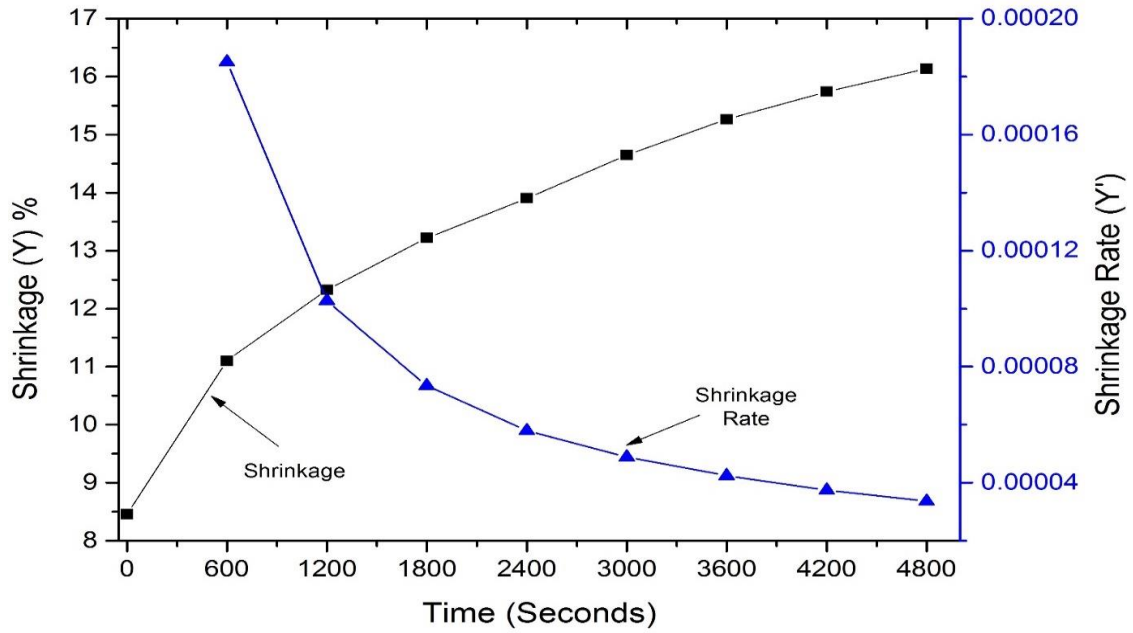
Figure 4.8: Measured shrinkage & shrinkage rate as a function of isothermal holding time at 1400 ^{0}C.
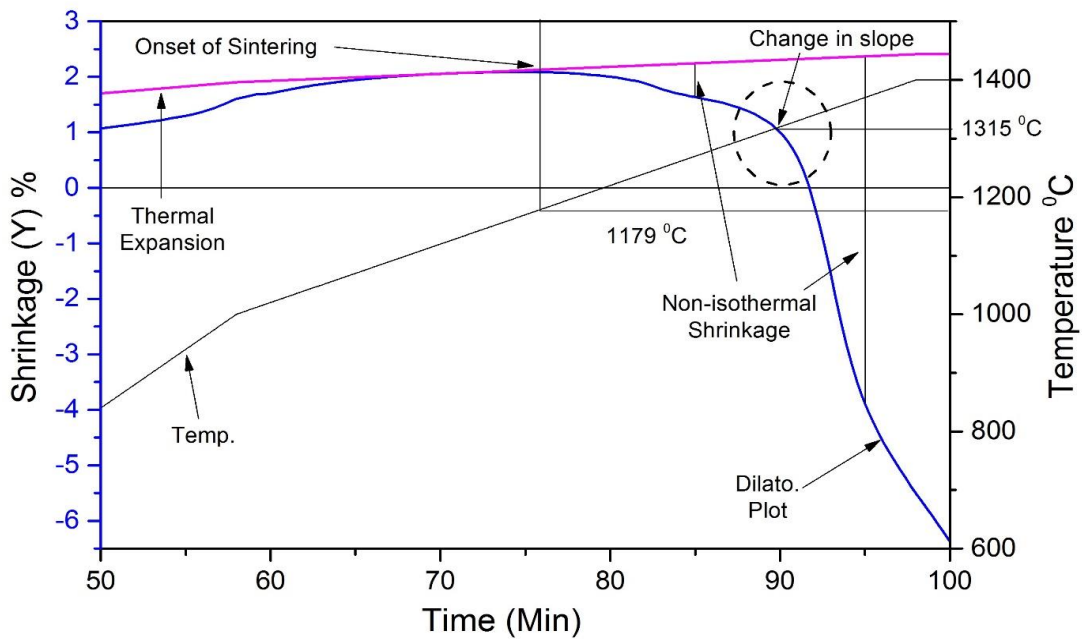
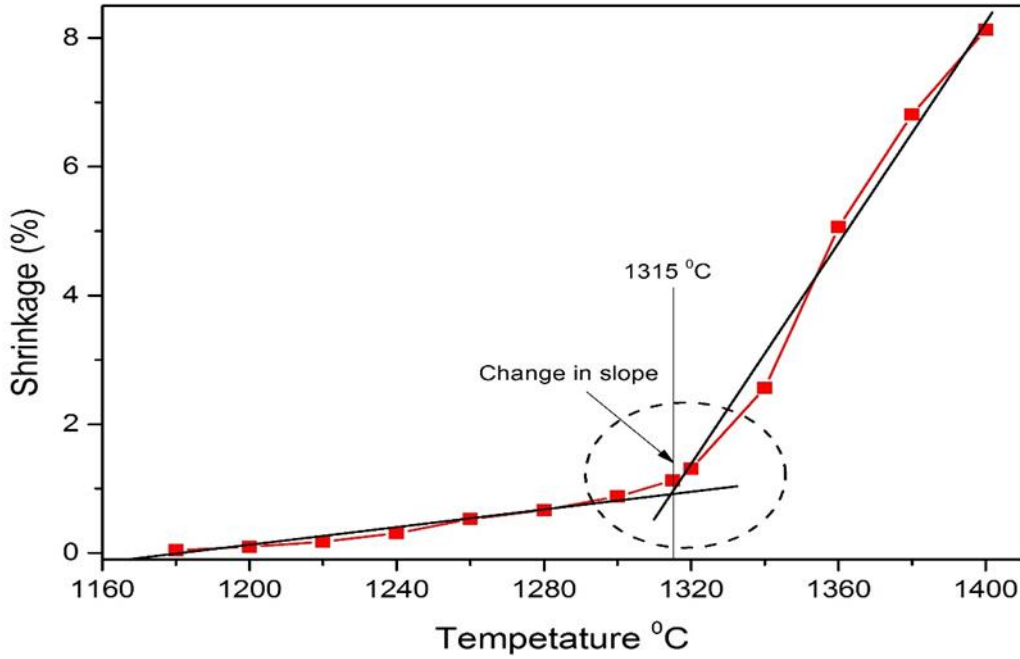Figure 4-9: Dilatometer plot of the CAC sample sintered up to 1400 ^{0}C for non-isothermal sintering.

Figure 4.10: Measured shrinkage as a function temperature for non-isothermal section up to 1400 ^0C.

4.3 Analysis of Sintering Kinetics

The activation energy(Q) has been estimated using equation (4.1) for sintering during a constant heating rate as reported by the Young and Cutler [34], modified by Han et al. [35] for non-isothermal sintering.

$$\ln\left(T^P \frac{dY}{dT}\right) = -\frac{Q}{(n+1)RT} + \ln C \qquad \qquad (4.1)$$

Y = Linear shrinkage ($\Delta L/L_n$)

T = Temperature in Kelvin

R = Universal gas constant (8.314 J mol^{-1}K^{-1})

C = Material dependent constant

n & P are constant, P = 1 & n = 0 (Viscous flow)

P = 3/2 & n = 1 (Volume diffusion)

P = 5/3 & n = 2 (Grain boundary diffusion)

Figure 4.11 shows the Arrhenius plot of ln ($T^p \frac{dY}{dT}$) vs 1/T for two different temperature range. Calculated activation energy have been tabulated in Table 5-1 for mechanisms. To estimate the diffusion parameter, Johnson's models [32] have been employed separately for the same data. Here the assumption was made that during pressureless sintering, mainly two mechanisms controls the process: (a) grain boundary diffusion and (b) volume

diffusion [32]. For sake of simplicity we have considered that each mechanism is contributing independently. Following models were used to estimate diffusion parameters of CAC samples:

For grain boundary diffusion;

$$Y^{2.06}\frac{dY}{dt} = \frac{2.14 Y \Omega b D_b}{kT r^4}$$

_____ (4.2)

And for volume diffusion,

$$Y^{1.04}\frac{dY}{dt} = \frac{5.34 Y \Omega D_v}{kT r^3}$$

_____ (4.3)

Where, Y = Linear Shrinkage

Υ = Surface free energy (37.3 x 10^{-3} J/m^2) [32]

T = Temperature in Kalvin

t = Time

Ω = atomic volume (molecular volume) (=4.532 x 10^{-29} m^3)

k = Boltzmann's constant 1.381 x 10^{-23} m^{2}kg/s^{2}K

r = Particle radius

D_v = Coefficient of volume diffusion

D_b = Coefficient of grain boundary diffusion

b = Grain boundary width

As it has been already observed that the as synthesized CAC is not of uniform size and having a range of particle size. Hence to overcome the errors due to particle size variation, values of D (diffusion coefficient) has been calculated for the range of particle size as shown in Figure 4.12 and Figure 4.13.

To measure the activation energy and frequency factors, ln (D_v) vs (1/T) for volume diffusion has been plotted for two different particle size of 8 and 12 μm as shown in Figure 4.14 (a). Similarly Figure 4.14 (b) shows ln (bD_b) vs (1/T) for grain boundary diffusion for the same particle size. Logarithmic form of Arrhenius relation [lnD = lnD$_0$ – (Q/RT)] was used for the calculation; where R is universal gas constant, D$_0$ is frequency factor and Q is activation energy. Results have been shown in Table 4.2.

It has been observed that activation energy is independent of particle size as expected [32] and frequency factor increases with particle size. This is because for coarse particles,

relatively higher diffusion rate of longer time is require to produce the same amount of shrinkage, than for smaller particles. However, as diffusion coefficients of individual element in Cr-Al-C ternary system are not yet available, any definite conclusion cannot be drawn at present. Also the increase in activation energy indicating towards the different diffusive species at higher temperature.
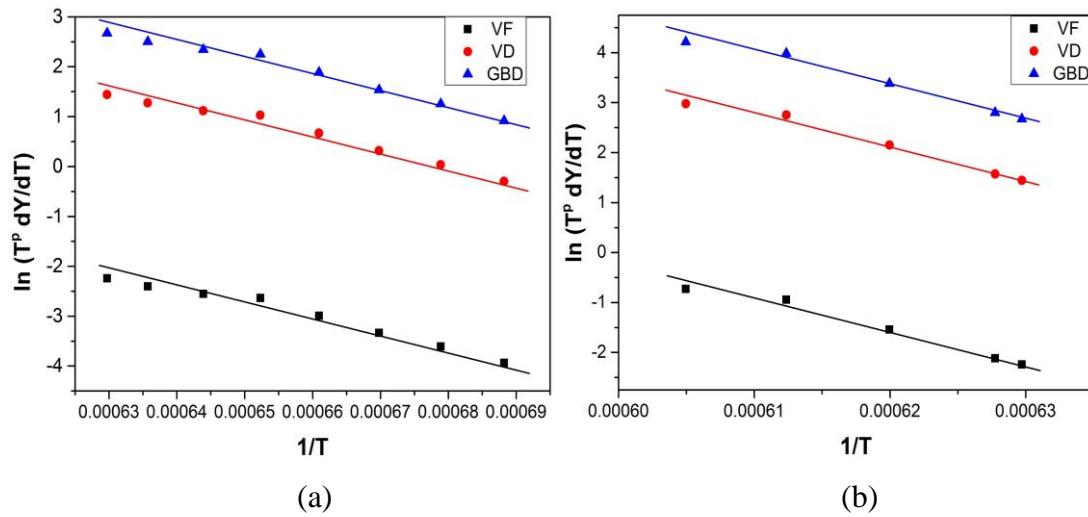

(a) (b)

Figure 4-11 - Arrhenius plots of equation (4.1) to estimate activation energy in two different temperature range (a) 1180-1315 ^{0}C and (b) 1315-1400 ^{0}C.

Table 4.1: Calculated activation energies by Young and Cutler's model.

	Activation Energy (kJ/mol)	
	1160-1315 ^{0}C	1315-1400 ^{0}C
Viscous Flow	242	449
Volume Diffusion	496	912
Grain Boundary Diffusion	750	1374

(a) **(b)**
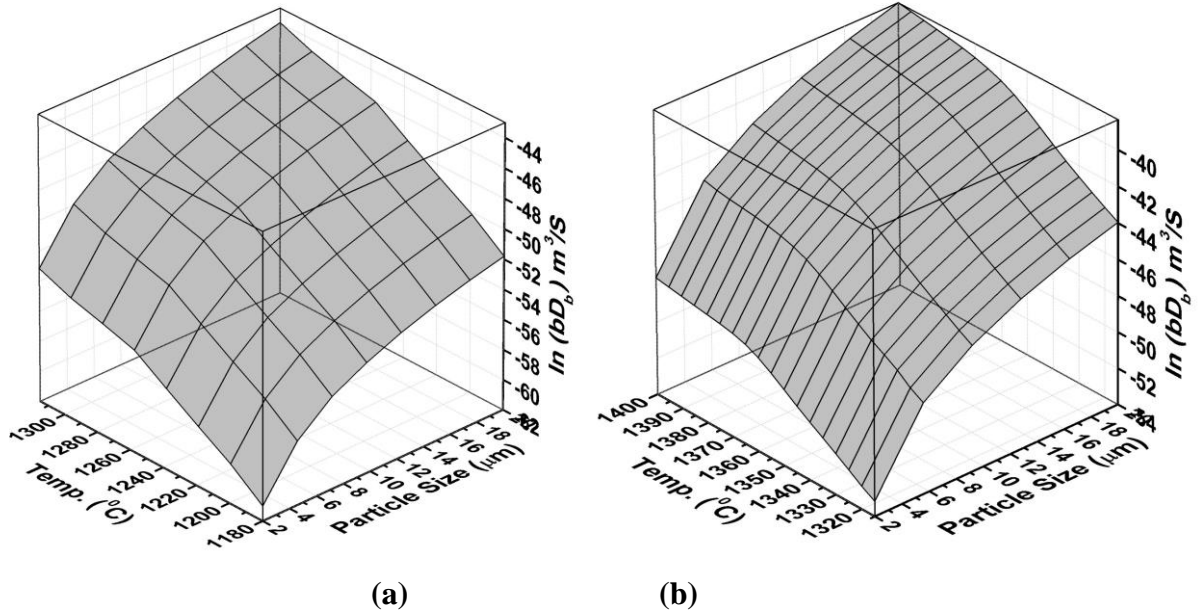
Figure 4.12: Grain boundary diffusion coefficient, ln (bD$_b$) as a function of temperature and particle size; (a) 1180-1315 ^{0}C and (b) 1315-1400 ^{0}C.

(a) **(b)**
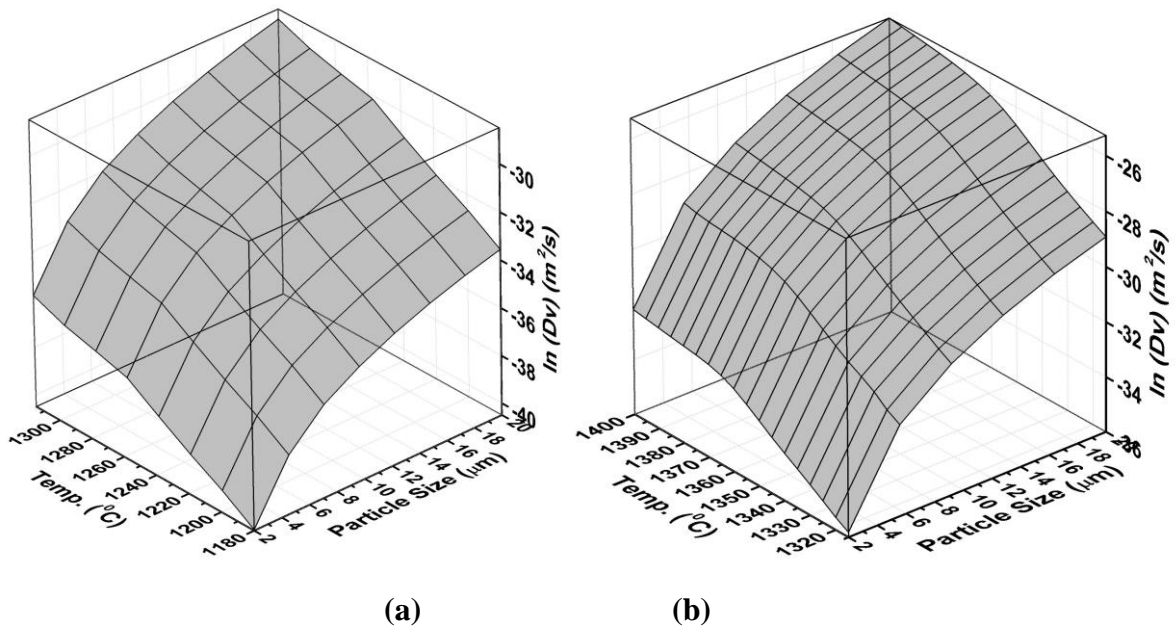
Figure 4.13: Volume diffusion coefficient, ln (D$_v$) as a function of temperature and particle size; (a) 1180-1315 ^{0}C and (b) 1315-1400 ^{0}C.
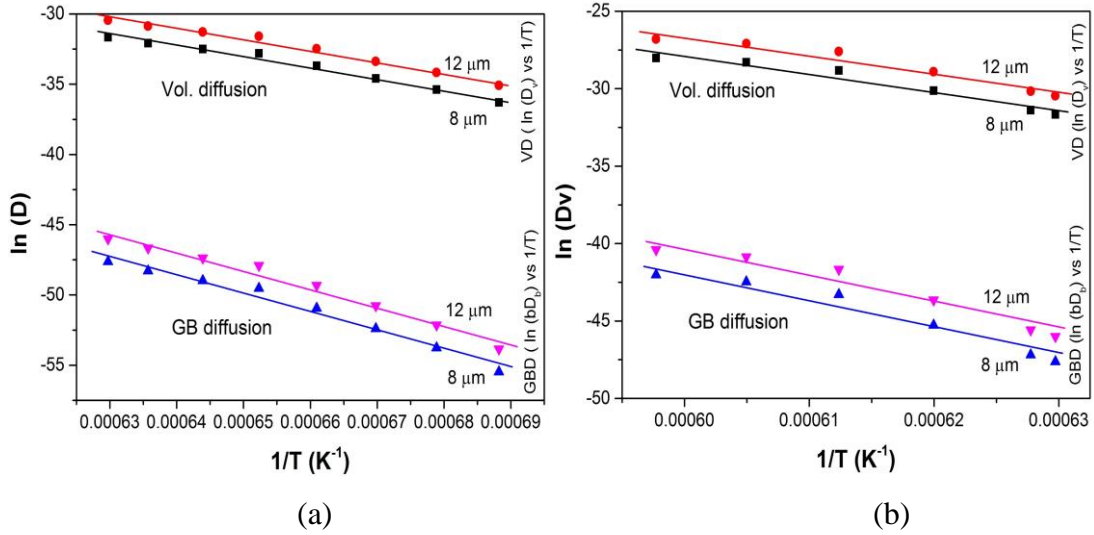
Figure 4.14: ln (D) vs 1/T to calculate activation energy & frequency factors for different particle size of 8 & 12 µm; (a) 1180-1315 ^{0}C and (b) 1315-1400 ^{0}C.

Table 4.2: Calculated activation energies and frequency factor of CAC using Johnson's models.

	Vol. Diffusion		GB Diffusion	
Particle Size	8 µm	12 µm	8 µm	12 µm
	Frequency Factor			
	D_{0v} (m^2/s)		bD_{0b} (m^3/s)	
1180-1315 ^{0}C	8.99 X 10^7	3.43 X 10^8	6.09 X 10^{15}	3.09 X 10^{16}
1315-1400 ^{0}C	2.70 X 10^{19}	9.13 X 10^{19}	1.63 X 10^{30}	8.27 X 10^{30}
	Activation Energy (kJ/mol)			
1180-1315 ^{0}C	685	685	1103	1103
1315-1400 ^{0}C	1006	1006	1543	1543

For further understanding, back scattered SEM images of polished sample has been taken to reveal any phase difference present. As it can be seen in Figure 4.15, some light region has been observed and point elemental analysis (EDS) of that region shows Al deficiency. Hence some carbides were certainly present with Cr$_2$AlC. Similar observation have also been reported by Xiao et al [36].

One possibility is the partial decomposition of Cr_2AlC at higher temperature due to the small amount of oxygen present. Xiao et al. [36] have reported the decomposition reaction at 1500 ^0C;

$$14Cr_2AlC + O2\ (g) \rightarrow Cr_{23}C_6 + Al_8Cr_5 + 3Al_2O_3 + 8CO\ (g)$$
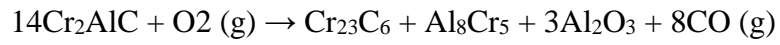
XRD pattern of the sintered sample as shown in Figure 4.16, confirms the presence of $Cr_{23}C_6$ phases, although Al_8Cr_5 and Al_2O_3 could not be detected.
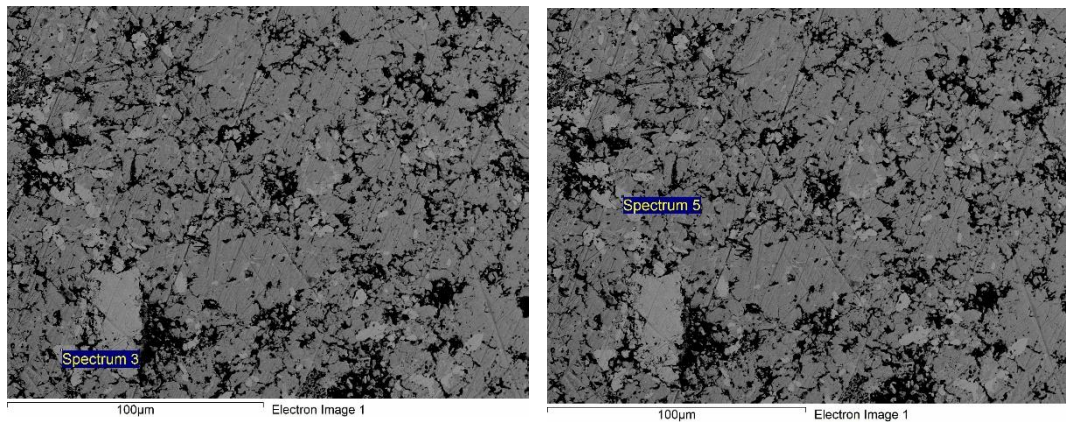
Element	Atomic %
C	31.3
Al	1.4
Cr	67.3

(a)

Element	Atomic %
C	30.15
Al	1.03
Cr	68.82

(b)

Figure 4.15: SEM backscattered image of CAC sintered at 1400 ^0C and EDS elemental analysis at two selected points (a) and (b).
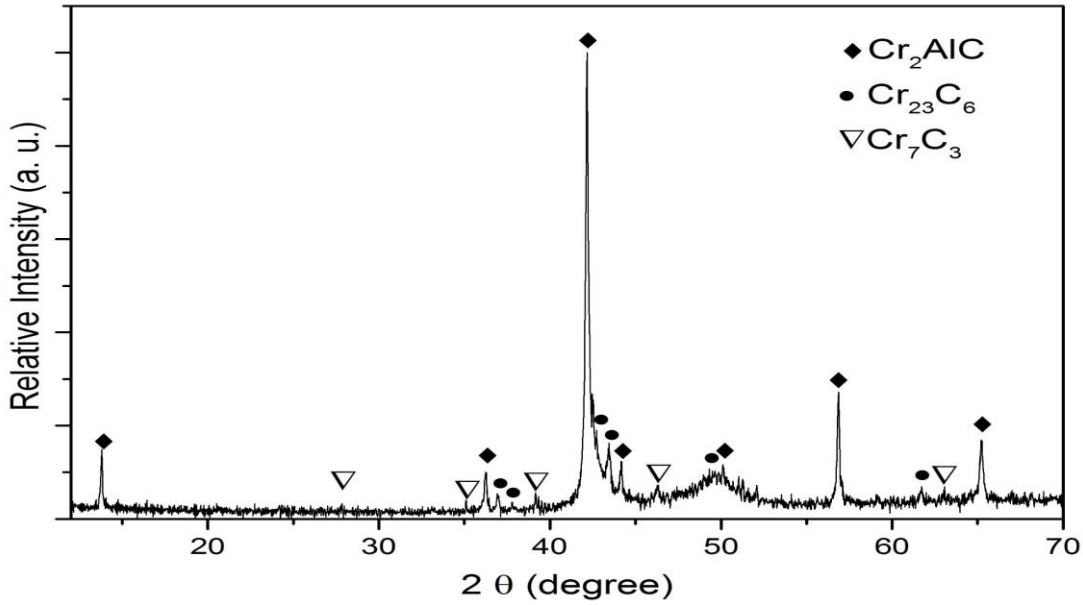
Figure 4.16: XRD pattern of CAC sample sintered at 1400 ^{0}C for 2 hours.

4.4 Effects of Zr addition on the sintering of CAC powder

Figure 4.17 shows the sintering curves of all CAC, CAC-1Zr, CAC-2Zr and CAC-5Zr samples together. With the addition of Zr huge expansion of samples before the actual onset of shrinkage have been observed. In all cases, expansion starts at around 850 ^{0}C and maximum at about 1110 ^{0}C.
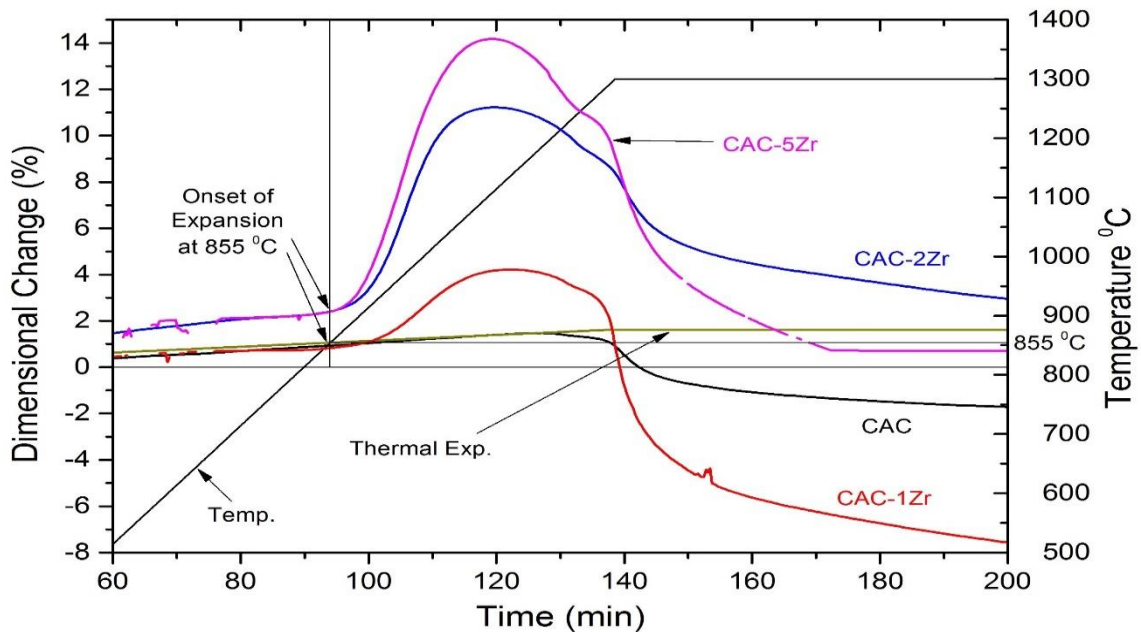

Figure 4.17: Dilatometer plots of CAC-Zr systems sintered at 1300 ^{0}C.

26

Figure 4.18 compares the maximum relative expansion for various amount of Zr added and Figure 4.19 shows the shrinkage from maximum expansion to the end of non-isothermal part of sintering curve. Increase in shrinkage after maximum expansion were observed with Zr content, but final sintered density (Table 4.3) shows the opposite results. This is mainly due to the large expansion prior to the onset of shrinkage. This expansion is may be contributed partially by the phase transformation of Zr metal. Zirconium has hcp crystal structure (α-Zr) up to 855 ^{0}C, which then transform to less dense bcc structure (β-Zr). Small amount of impurities, particular oxygen strongly affect the transformation temperature [36]. Expansion may also partially contributed due to the formation of Cr-Al-Zr ternary phase, but this needs further investigations.
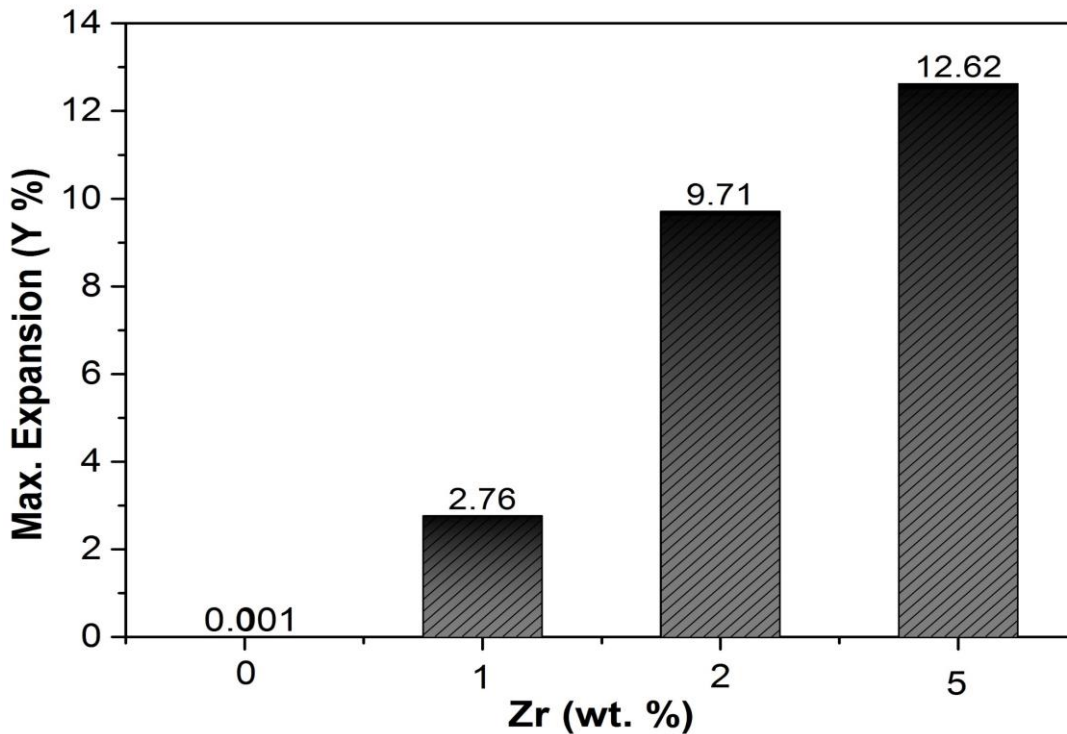
Figure 4.18: Maximum relative expansion observed during dilatometer sintering for all CAC-Zr samples.
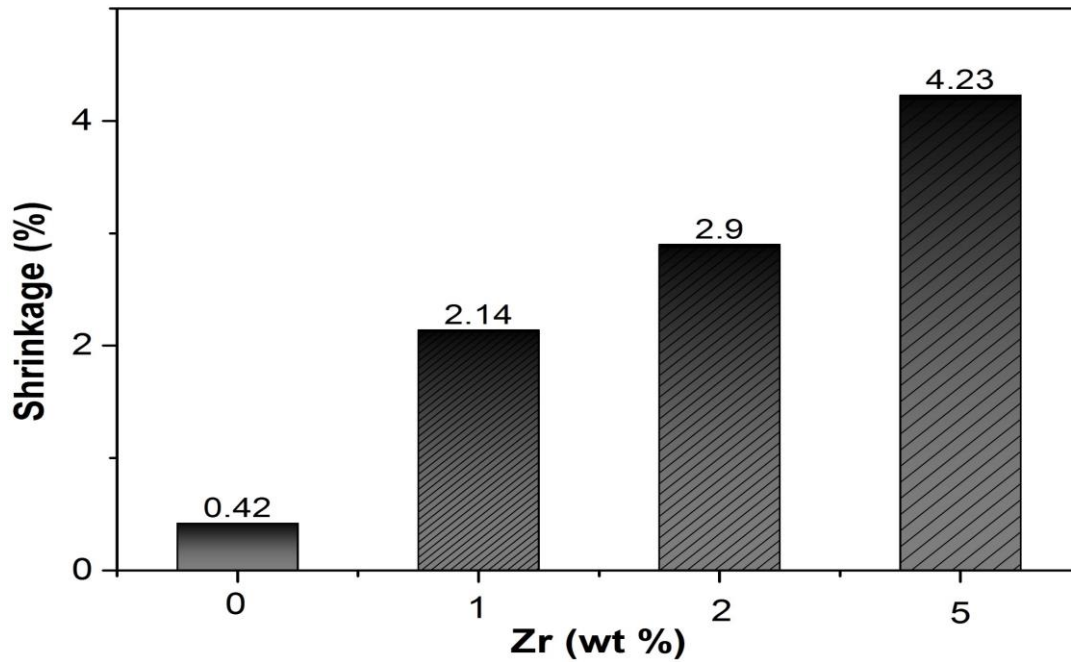
Figure 4.19: Shrinkage from maximum expansion observed during dilatometer sintering for all CAC-Zr samples.

Table 4.3: Relative Green & sintered density measured for all dilatometer sintered CAC-Zr samples.

	CAC	CAC-1Zr	CAC-2Zr	CAC-5Zr
Green Density	62.10%	62.80%	64.10%	63.30%
Sintered Density	73.60%	70.70%	63.20%	63.80%

To further investigate the effect of Zr on the CAC, SEM images have been taken for some of the fracture surfaces. EDS elemental analysis have also been carried out for selected area of few samples. Figure 4.20 (a), (b), (c) and (d) shows CAC, CAC-1Zr, CAC-2Zr and CAC-5Zr at 5kX whereas (e), (f), (g) and (h) respectively at 10 kX magnification . Figure 4.21 (a) shows image of CAC-1Zr and elemental maps of Cr, Al and Zr for some image. Similarly Figure 4.21 (b) shows the image of CAC-5Zr and its elemental mappings. Elemental mapping is showing uniform distribution of Zr except for very few places and it was difficult to derive some conclusion. With increased amount of Zr content, pores in CAC lamina found to be increased as can be seen in Figure 4.20 (f), (g) and (h). Elemental mapping shows the uniform distribution of Zr along with Cr and Al except for very few

points. This is possibly because of atomic diffusion of Zr at higher temperature due to chemical gradient. XRD (Figure 4.22) shows somewhat higher amount of binary carbides along with small amount Cr-Al intermetallic, which may be indicating some decomposition during sintering. Amount of binary carbides and $AlCr_2$ increase with Zr content, indicates towards the possible decomposition, due to higher amount of Zr.

As shown in figure 4.23, DSC analysis of CAC-Zr samples do not detects any apparent change in profile with respect to pure CAC. Three major endothermic peaks attributes probably to the melting of some Cr-Al intermetallic compounds. Hence the reason for huge expansion of CAC in the presence of Zr is still not very clear and require further investigations.
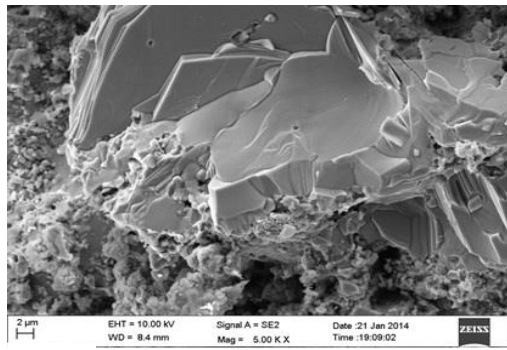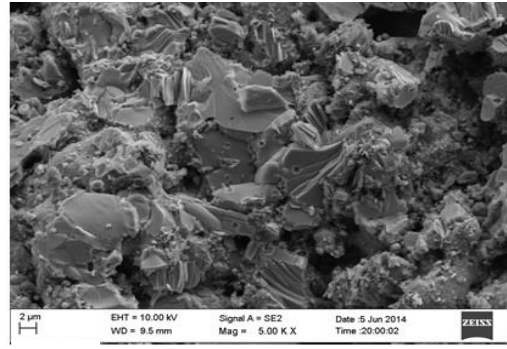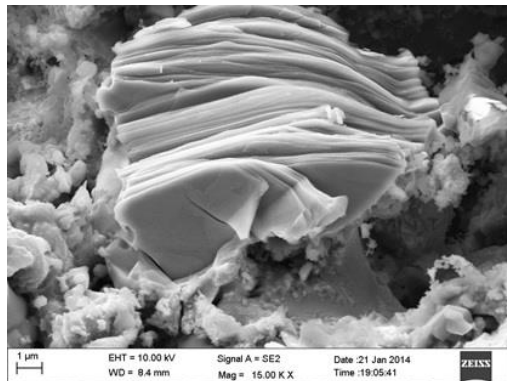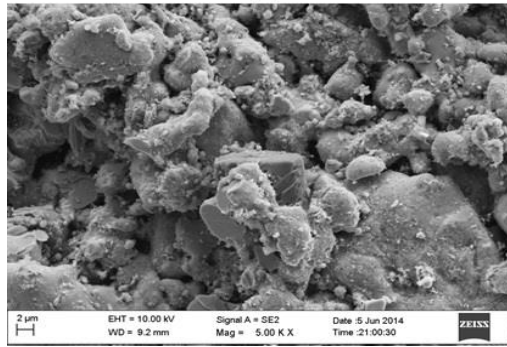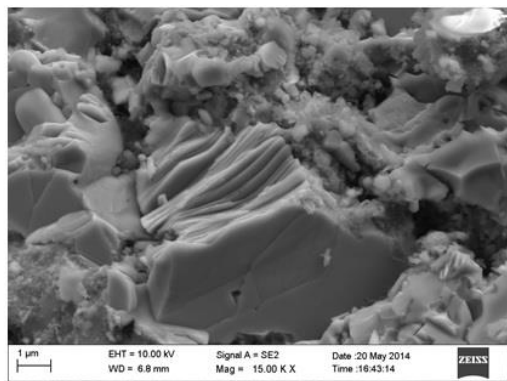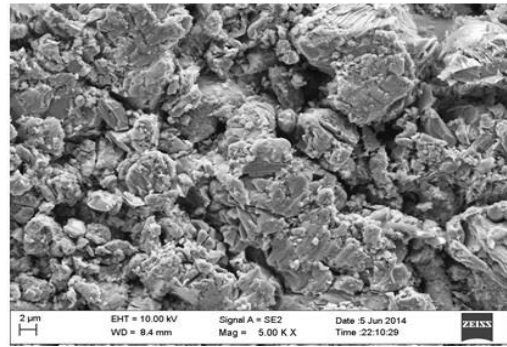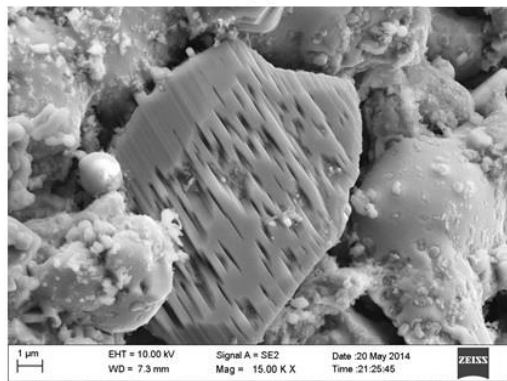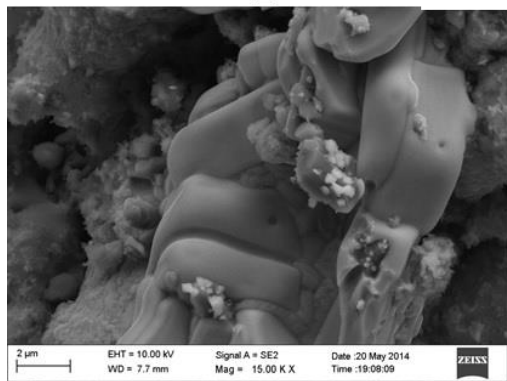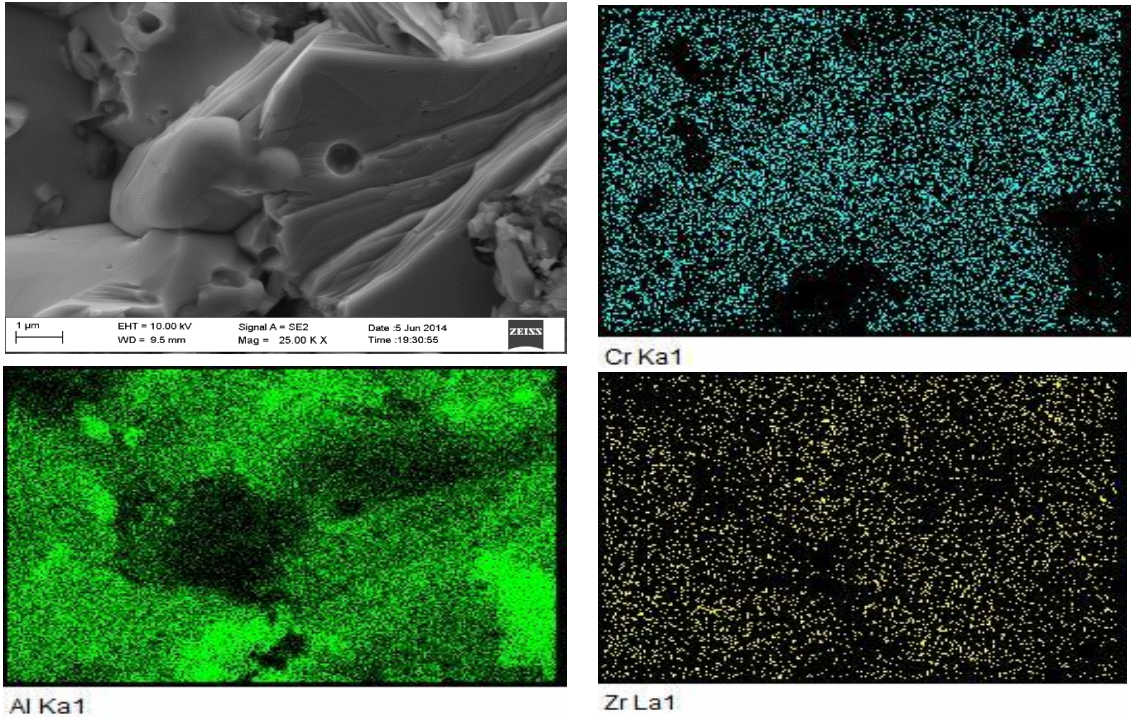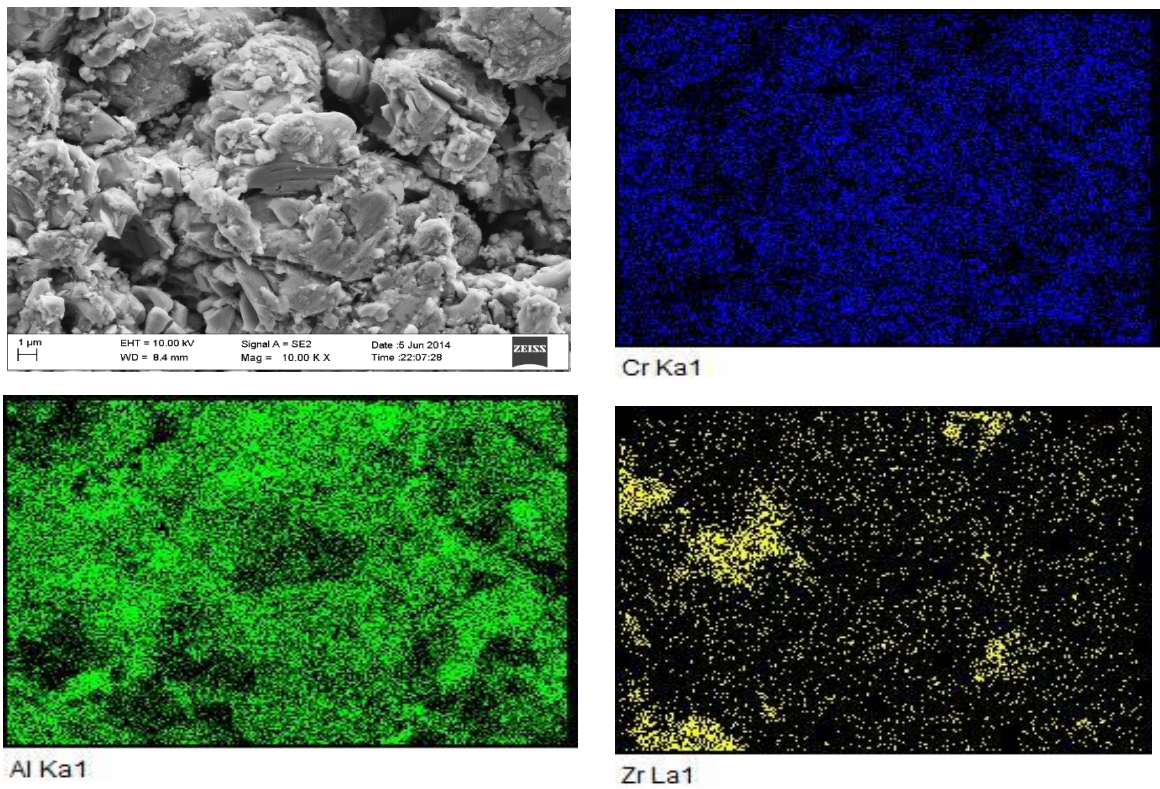
Figure 4.20: SEM images of fracture surface of sintered CAC-Zr samples.

(a)

(b)

Figure 4.21: Elemental mapping of selected area of some sintered CAC-Zr samples (a) CAC-1Zr & (b) CAC-5Zr).
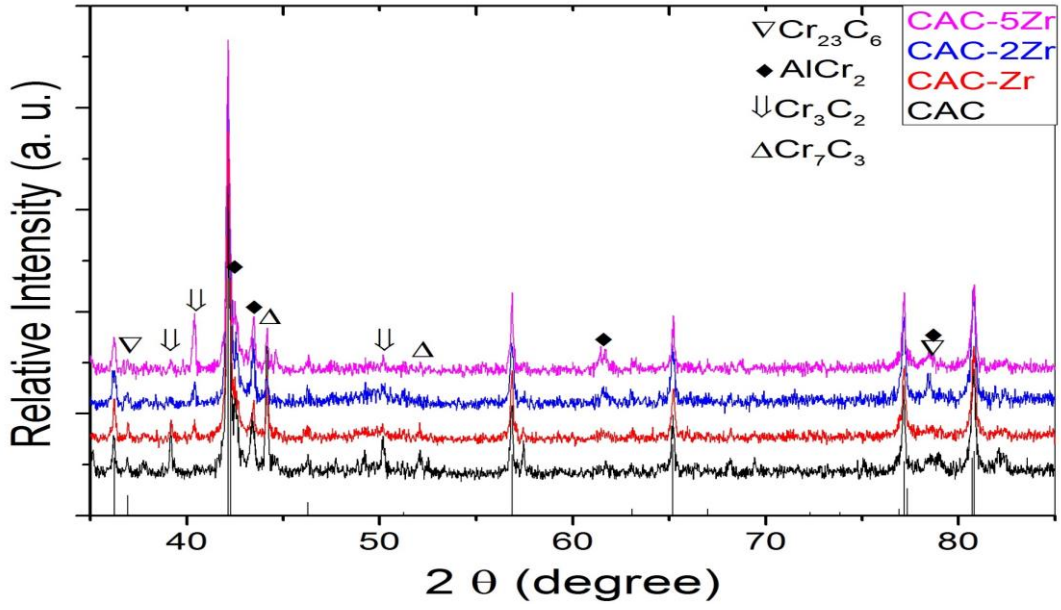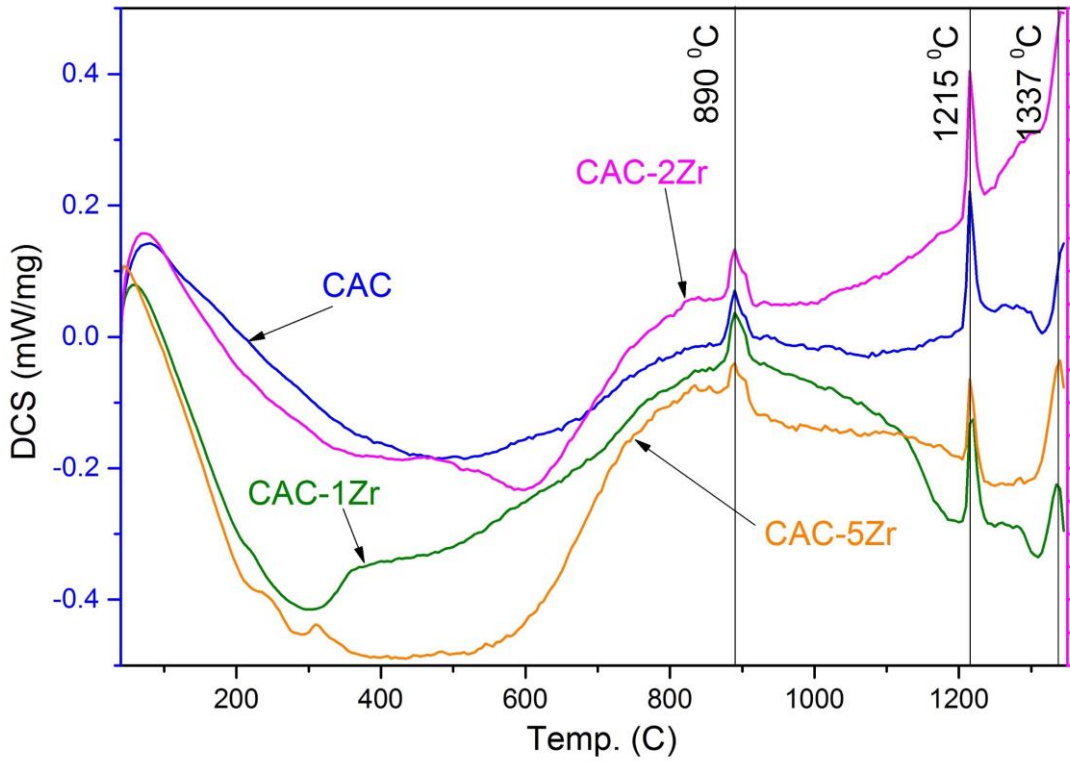
Figure 4.22: XRD of all CAC –Zr samples sintered at 1300 ^{0}C.

Figure 4.23: DSC plots of all CAC-Zr samples.

Chapter 5
Conclusions

Sintering behavior of Cr_2AlC powder as well as effect of sintering aids (zirconium powder) have been studied in the present work using dilatomeric sintering experiments. Experimentally obtained data were analyzed with the help of classical sintering models. Non-isothermal sintering kinetics data were analyzed using Young and Cutler's as well as Johnson's models. Dilatometer curve shows drastic change in shrinkage plot at 1315 ^{0}C, and hence data has been divided in two different temperature range. Activation energies for volume diffusion, grain boundary diffusion and viscous flow have been estimated. Addition of zirconium powder causes large expansion of Cr_2AlC compact before the onset of sintering. The reason for this expansion is not very much clear. However after expansion samples shows rapid shrinkage. Role of Zr in Cr_2AlC system is not fully understood and hence it requires further investigation.

References

[1] M. W. Barsoum, "The $M_{n+1}AX_n$ Phases: A New class of Solids; Thermodynamically Stable Nanolaminates", Progress in Solid State Chemistry 28 (2000) 201-281

[2] X. K. Qian, "Methods of MAX phase synthesis and densification – 1", Advances in science and technology of $M_{n+1}AX_n$ Phases, Woodhead Publishing 2012

[3] M. W. Barsoum and Miladin Radovic, "Elastic and mechanical properties of MAX phases", Annual Review of Materials Research 41 (2011) 195-227

[4] M. W. Barsoum and T. El-Raghy, "Synthesis and Characterization of Remarkable Ceramic: Ti_3SiC_2", Journal of American Ceramic Society 79 (1996) 1953

[5] B. B. Panigrahi, M-C Chu, Y-I Kin, S-J Cho and J. J. Gracio, "Reaction Synthesis and Pressureless Sintering of Cr_2AlC Power", Journal of American Ceramic Society 93 [6] (2010) 1530-1533

[6] J. C. Schuster, H. Nowotny and C. Vaccaro, "The Ternary Systems: Cr-Al-C, V-Al-C and Ti-Al-C and the Behaviour of the H-phases (M_2AlC)", Journal of Solid State Chemistry 32 (1980) 213

[7] Z J Lin, Y. C. Zhou, M. S. Li and J. Y. Wan, "In-situ hot pressing/solid-liquid reaction synthesis of bulk Cr_2AlC", Z. Metallkd. 96 (2005) 291

[8] Zhijun Lin, M. Zhuo, Y. Zhou, M. Li and J. Wang, "Atomic scale characterization of layered ternary Cr_2AlC ceramic", Journal of Applied Physics 99 (2006) 076109

[9] H. J. Yang, Y. T. Pei and J. Th. M. De Hosson, "Oxide-scale growth on Cr_2AlC ceramic and its consequence for self-healing", Scripta Materialia 69 (2013) 203-206

[10] T. H. Scabarozi, S. "Amini, O. Leaffer, A. Ganguly, S. Gupta, W. Tambussi, S. Clipper, J. E. Spanier, M. W. Barsoum, J. D. Hettinger and S. E. Lofland, "Thermal expansion of selected $M_{n+1}AX_n$ (M = early transition metal, A = A group element, X = C or N) phases measured by high temperature X-ray diffraction and dilatometry", Journal of Applied Physics 105 (2009) 013543

[11] J. M. Schneider, Z. Sun, R. Mertens, F. Uestel and R. Ahuja, "Ab initio calculations and experimental determination of the structure of Cr_2AlC", Solid State Communication 130 (2004) 445-449

[12] ASM Handbook, Volume – 7, Powder Metal Technologies and Applications

[13] ASM Handbook, Volume – 3, Alloy Phase Diagrams

[14] Zhou, "Methods of MAX-phase synthesis and densification – II" Advances in science and technology of $M_{n+1}AX_n$ Phases, Woodhead Publishing 2012

[15] Randall M. German, "Powder Metallurgy Science", Metal Powder Industries Federation

[16] Barsoum M. W., El-Raghy T., "Synthesis and characterization of a remarkable ceramic: Ti3SiC2", Journal of American Ceramic Society, 79 (1996) 1953-1956

[17] Tzenov N. V., Barsoum M. W., "Synthesis and characterization of Ti3AlC2", Journal of American Ceramic Society 83 (2000) 825-832

[18] Y. C. Zhou, Z. Sun, S. Chen, and Y. Zhang, "In situ hot pressing solid–liquid reaction synthesis of dense titanium silicon carbide bulk ceramics", Mater Res Innovation, 2 (1998) 142-146

[19] Z-M. Sun, S. Yang and H. Hashimoto, "Ti_3SiC_2 powder synthesis", Ceramics International 30 (2004) 1873-1877

[20] B. Hallstedt, D. Music and Z. Sun, "Thermodynamic evaluation of Al-Cr-C system", International Journal of Materials Research 97 (2006) 539-542

[21] W. B. Tian, P-L Wang, Y-M Kan, G-J Zhang, Y-X Li and D-S Yan, "Phase formation sequence of Cr_2AlC ceramics starting from Cr-Al-C powders", Materials Science and Engineering-A 443 (2007) 229-234

[22] Randall M. German, "Sintering Technology", CRC Press, 1996

[23] N. F. Gao, J. T. Li, D. Zhang and Y. Miyamota, "Rapid synthesis of dense Ti_3SiC_2 by spark plasma sintering", Journal of European Ceramic Society 22 (2002) 2365-2370

[24] Zhu J. Q. and Mei B. C., "Effect of aluminium on synthesis of Ti_3SiC_2 by spark plasma sintering (SPS) from elemental powders", Journal of Mater Synth Process 10 (2002) 353-358

[25] W. B. Zhou, B. C. Mei, J. Q. Zhu and X. L. Hong, "Rapid synthesis of Ti2AlC by spark plasma sintering technique", Materials Letters 59 (2005) 131-134

[26] W-B Tian, K. Vanmeensel, P. Wang, G. Zhang, Y. Li, J. Vaeugels, and O. Van der Biest, "Synthesis and characterization of Cr_2AlC ceramics prepared by spark plasma sintering", Materials Letters 61 (2007) 4442-4445

[27] W-B Tian, Z-M Sun, Y. Du and H. Hashimoto, "Synthesis reaction of Cr_2AlC from $Cr-Al_4C_3$-C by pulse discharge sintering", Materials Letters 62 (2008) 3852-3855

[28] W-B Tian, P-L Wang, Y-M Kan and G-J Zhang, "Cr_2AlC powders preparation by molten salt method", Journal of Alloys and Compounds 461 (2008) L5-L10

[29] B. B. Panigrahi, J. J. Gracio, M-C Chu, S-J Cho and N. Subba Reddy, "Powder synthesis, Sintering Kinetics, and Nickel-Activated Pressureless Sintering of Ti_3AlC_2", International Journal of Applied Ceramic Technology 7 (2010) 752-759

[30] B. B. Panigrahi, N. Subba Reddy, A. Balakrishnan, M-C Chu, S-J Cho and J. J. Gracio et al. "Nickel assisted sintering of Ti_3SiC_2 powder under pressureless conditions", Journal of Alloys and Compounds 505 (2010) 337

[31] Z. Su, S. Zeng, J. Zhou and Z. Sun, "Synthesis and characterization of Cr2AlC with nanolaminated particles" Chinese Science Bulletin 59 (2014) 3266-3270

[32] B. B. Panigrahi, "Prediction of Diffusion Coefficient of Ti_3SiC_2 and Cr_2AlC Ceramics Using Sintering Models", Transaction of Powder Metallurgy Association of India 38 (2012) 71-75

[33] B. B. Panigrahi, "Evaluation of dimensional change from as received dilatometer sintering plot", Materials Science and Technology 23 (2007) 103-107

[34] W. S. Young and I. B. Cutler, "Initial sintering with constant rate heating", Journal of American Ceramics Society 53 (1970) 659-663

[35] J. Han, A. M. R Senos and P. Q. Mantas, "Nonisothermal sintering of Mn doped ZnO", Journal of European Ceramics Society 19 (1999) 1003-1006

[36] L-O Xiao, S-B Li, G. Song and W. G. Sloof, "Synthesis and thermal stability of Cr_2AlC", Journal of European Ceramic Society 31 (2011) 1497-1502

[37] ASM Handbook, Volume – 2, Properties of Selected Nonferrous Alloys and Special Purpose Materials

[38] Michel Barsoum, "The MAX Phases: Unique New Carbides and Nitride Materials", American Scientist 89 (4) (2001) 334

[39] W-B Tian, P-L Wang, Y. Liu, M-H Cao, and Shi-Xi Ouyang, "Mechanical Properties of Cr2AlC Ceraminc", Journal of American Ceramic Society 90 (2007) 1663-1666

[40] C. W. Corti, "Sintering aids in powder metallurgy", Platinum Metals Review 30 (1986) 184-195